Colloid and Polymer Science (2018) 296:781–798
https://doi.org/10.1007/s00396-018-4297-8

ORIGINAL CONTRIBUTION

Surface dilational viscoelasticity of aqueous surfactant solutions by surface quasi-elastic light scattering

Shusaku Ueno[1] · Yuichi Takajo[1] · Shunsuke Ikeda[1] · Ryo Takemoto[1] · Yosuke Imai[2] · Takanori Takiue[2] · Hiroki Matsubara[1] · Makoto Aratono[1]

Received: 2 January 2018 / Accepted: 25 February 2018 / Published online: 10 March 2018

Abstract

We investigated the surface dilational viscoelasticities of aqueous solutions of dihexanoyl-phosphastidylcholine (DC_6PC) and dioctanoyl-phosphastidylcholine (DC_8PC), dodecyltrimethylammonium bromide (DTABr) and DTABr and sodium bromide (NaBr), dodecyltrimethylammonium tetrafluoroborate ($DTABF_4$) and bisdodecyltrimethylammonium sulfate (DTA_2SO_4), and nonionic surfactants with oxyethylene units ($C_{10}E_5$). We measured surface quasi-elastic light scattering (SQELS) spectra and analyzed the solutions by both surface rheological and phenomenological fitting approaches. For the DC_6PC-DC_8PC mixture, the electrocapillary wave (ECW) method was also applied. The molecular interactions between DC_8PC and DC_6PC in the adsorbed film clearly influenced the relaxation process on the order of several milliseconds (ECW). However, the effects were less influential on the order of several hundreds of microseconds (SQELS). The characteristic frequencies for relaxation owing to the staggered structure formation likely occurred in the range from 150 to 300 Hz. The dilational elasticity at 250–400 kHz of DTABr suggested that the main relaxation process influencing the dilational properties was neither diffusion of surfactants from the bulk phase to the subsurface nor an adsorption-desorption of surfactant ions between the adsorbed layer and subsurface. However, the diffusion of counterions between the Stern and diffuse layers occurred on a time scale of several microseconds. Studies of $C_{10}E_5$ suggested that the relaxation process captured by the SQELS studies was neither related to surfactant diffusion nor surfactant reorientation, but rather was likely to be a relaxation process where distortion of the hydration sphere and/or hydration-dehydration to/from the hydration sphere was caused by diffusion of water molecules.

Keywords Surface tension · Surfactants · Adsorption · Dilational elasticity · Relaxation · Light scattering

This manuscript reports that the surface quasi-elastic light scattering (SQELS) incorporated with both surface rheological and phenomenological fitting approaches was applied to determine the surface dilational viscoelasticities of aqueous solutions of DC6PC+DC8PC, DTABr, DTABr +NaBr, DTABF4, DTA2SO4, and C10E5.The effects of salt concentration (electrical double layer) and counter ion on the dilational viscoelasticity were carefully determined and demonstrated. It is interesting to be further verified that the negative values of surface dilational viscosity were somehow closely related to the resonance between the transversal and dilational waves. The manuscript is well organized and prepared. These experimental data are new and important to explore the physical insight of surface dilational viscoelasticity. This manuscript is suitable to be published in the Colloid and Polymer Science.

✉ Makoto Aratono
aratono@chem.kyushu–univ.jp

[1] Department of Chemistry, Faculty of Science, Kyushu University, 744 Motooka, Nishi-ku, Fukuoka 819-0395, Japan

[2] Faculty of Arts and Science, Kyushu University, 744 Motooka, Nishi-ku, Fukuoka 819-0395, Japan

Introduction

Surface viscoelasticity represents the rigidity and fluidity of surface layers and is defined as the restoring force, which works against deformation of the surface layer. This topic has been well reviewed [1–7] because of its theoretical and practical importance. For example, interfacial rheology often plays an important role in understanding the dynamics of surfactant layers that are related to emulsion stability [8], collapse of foam films [9], plate coating [10], and membrane systems [11]. The interfacial rheology of polymer films has been intensively researched in recent years [4, 12, 13], because of its practical importance for industrial applications; however, further studies of the rheology of films of adsorbed surfactants over a wide range of frequencies of surface perturbation are required to consolidate the basic concepts of interfacial rheology and the applicability of certain proposed models.

There are shear and dilational parameters for surface viscoelastic properties. However, the magnitude of the former is typically smaller than that of the latter by several orders [14]; thus, we focus our investigation on the dilational properties. For adsorbed films of soluble surfactants, the dilational viscoelastic properties are strongly dependent on the perturbation frequency, and thus, several experimental methods have been used to clarify surface dilational properties at different frequencies: the combination of oscillating drops and bubbles can be used to access data in a frequency range between 10^{-3} and 100 Hz. The capillary wave damping method can be used to study frequencies up to 1000 Hz and the surface quasi-elastic light scattering (SQELS) method can be used to assess to those up to approximately 1 MHz [6]. The oscillating drop method enabled the surface viscoelasticity of aqueous solutions of surfactants to be studied at low frequencies by Miller et al. [6, 15, 16], from which information was obtained on slower dynamic processes, such as bulk diffusion and adsorption barriers. The electrocapillary wave (ECW) method has been used for studies at intermediate frequency regions (~kHz) for cationic surfactants, and the viscoelastic coefficients have been determined by applying dispersion equations and models describing the adsorption state and processes [17, 18]. Furthermore, surface light scattering techniques at higher frequencies (between 5 and several hundred kHz) have been applied to different kinds of surfactants and revealed that negative surface dilational viscosities are often evaluated [17, 19–21].

In this study, we focus on the dilational viscoelasticity of adsorption layers in the high frequency region with the use of the surface quasi-elastic light scattering (SQELS) method. SQELS is based on ripplons generated by the thermal motion of constituent molecules at the surface and is thus advantageous as non-perturbative and non-contact method. The SQELS method features certain experimental peculiarities, in that the spectrum of scattered light features considerable instrumental broadening and becomes less applicable for extremely large surface viscoelasticities. However, these issues are respectively resolved by calibrating the SQELS equipment with pure water and choosing an appropriate accessible region of the surface viscoelastic parameters from the SQELS [12]. The other difficulty of the SQELS method is the theoretical complexity of air/aqueous solution surfaces. The dilational parameters should be derived from analysis of the experimentally detected transversal waves (capillary waves) through the dispersion equation, which often provides an unrealistic negative viscosity. Although there are some theoretical approaches to resolving the problem of negative viscosity, this issue has yet to be clarified. For example, Hennenberg et al. explained the physical reasons for improving the van den Temple-Lucassen theory by taking into account contributions from surface deformation [22], and Monroy et al. proposed a new dispersion equation that accounts for internal coupling between capillary and dilational modes, which leads to non-anomalous dilational viscosities [23].

First, we used SQELS to study the ripplon frequency at approximately 250 kHz of a short-chain phospholipid mixture of dihexanoyl-phosphatidylcholine (DC_6PC) and dioctanoyl-phosphatidylcholine (DC_8PC). This mixture was chosen because both storage and loss modulus values at approximately 0.2 kHz by the ECW show a maximum near the surface composition of the minimum of the excess Gibbs energy of adsorption, which can be attributed to a staggered arrangement of the mixed adsorbed film [24]. Thus, the effects of the perturbation frequency on the surface viscoelasticity will be extracted by comparing the SQELS results with those from ECW. For this purpose, we also performed some ECW experiments on the DC_6PC and DC_8PC mixtures at different frequencies from 0.2 kHz.

For a better understanding of the surface viscoelasticity from SQELS, we used aqueous solutions of different types of surfactant: (A) dodecyltrimethylammonium bromide (DTABr), (B) DTABr in the presence of sodium bromide (NaBr), (C) dodecyltrimethylammonium tetrafluoroborate ($DTABF_4$) and bis-dodecyltrimethylammonium sulfate (DTA_2SO_4), and (D) pentaethyleneglycol monodecyl ether ($C_{10}E_5$). DTABr was chosen because its equilibrium surface properties [25, 26] and dilational viscoelastic properties [17, 18, 27, 28] have been relatively well investigated. Comparing (A) with (B), we might gain information on the effects of the electrical double layer on the dilational viscoelasticity. Comparing (A) with (C), we might gain insight into the influence of the degree of counter ion binding to the surfactant ion on dilational viscoelasticity because the (A) and (C) systems contain the same surfactant ions but different counterions. Previous studies by surface tension [29–32] and total reflection X-ray absorption fine structure (TRXAFS) [33, 34] measurements have clarified that differences in the dehydration energy of counterions and their ionic atmosphere affect the surface density of adsorbed films. Thus, the SQELS measurement is expected to enable examination of how these factors influence the surface viscoelasticity of adsorbed films. Furthermore, (D) was chosen because it is nonionic, and its hydrophilic chain is considerably hydrated; thus, we might better understand the influence of water molecules on the dilational viscoelasticity.

This paper is constructed as follows. In the "Materials and methods" section, the materials and the thermodynamic equations for the surface tension analysis [35] are described and the SQELS apparatus is explained. Next, the theoretical background for evaluating the surface viscoelasticity parameters, that is, the dispersion relation [36], is presented and the two analytical methods of analyzing the SQELS spectrum, i.e., the surface rheological and phenomenological fitting analysis, are described. In the "Results and discussion" section, first, SQELS and ECW studies of short-chain phospholipid

mixtures are presented and then the surface dilational elasticities from the SQELS method are explained and examined, where the Lucassen and van den Temple model [17, 37–39] is introduced to understand the adsorption dynamics from the viewpoint of viscoelasticity. Finally, we briefly mention the dependence of the damping coefficients on the coupling of dilational and capillary waves.

Materials and methods

Materials

1,2-Dihexanoyl-*sn*-glycero-3-phosphocoline (DC_6PC) and 1,2-dioctanoyl-*sn*-glycero-3-phosphocoline (DC_8PC) were purchased from Avanti Polar Lipids (USA) and used without further purification. DTABr (99%) purchased from Wako Pure Chemical Industries (Japan) was purified by recrystallizing it five times from the acetone/ethanol mixture (volume ratio = 5/1). NaBr (99.9%) purchased from Aldrich Chemical Co. Inc. (USA) was used without further purification. $DTABF_4$ was synthesized by exchanging Br^- ions for BF_4^- ions by adding an equimolar amount of sodium tetrafluoroborate ($NaBF_4$) into an aqueous solution of DTABr, followed by recrystallization twice from water. The $NaBF_4$ (98%) purchased from Kanto Kagaku Co., Ltd. (Japan) and was recrystallized once from water and then baked at 170 °C for 7 h under reduced pressure. DTA_2SO_4 was synthesized by exchanging Br^- ions for SO_4^{2-} ions by adding a half molar amount of Ag_2SO_4 into an ethanol solution of DTABr. The Ag_2SO_4 (99.5%) was purchased from Wako Pure Chemical Industries and used without further purification. The ethanol solution was ultra-sonicated for 9 h and then AgBr precipitates were removed with 0.2-μm pore filters. A white solid salt was yielded from the filtrates, which was then recrystallized twice from methanol/acetone mixtures (volume ratio = 1/4) and dried at 90 °C under reduced pressure. The final product contained a small amount of water, which was estimated to be about 1 wt% with a Kahl–Fischer moisture meter and taken into account in the sample preparation. $C_{10}E_5$ was purchased from Bachem AG (Switzerland) and purified by the three-phase extraction technique [40]; the weight ratio of water/hexane/surfactant was 42.5/42.5/15. Ultrapure MilliQ water was used to prepare all surfactant solutions.

The purity of these materials was confirmed by observing that the surface tension of aqueous solutions reached a constant value that agreed with literature values and did not change over time. Furthermore, for all surfactants, it was confirmed that the surface tension vs. molality curves did not show a minimum around the critical micelle concentrations.

Thermodynamic equations for surface tension analysis

The surface tension was analyzed as follows. Let us consider a system composed of air and aqueous solution of DTABr and NaBr. The total differential of the surface tension γ is expressed as a function of temperature T, pressure p, and the the electrochemical potential of the ions α, $\tilde{\mu}_\alpha$ ($\alpha = \mathrm{DTA}^+, \mathrm{Na}^+, \mathrm{Br}^-$) by

$$\mathrm{d}\gamma = -s^{\mathrm{H}}\mathrm{d}T + v^{\mathrm{H}}\mathrm{d}p - \Gamma^{\mathrm{H}}_{\mathrm{DTA}^+}\mathrm{d}\tilde{\mu}_{\mathrm{DTA}^+} - \Gamma^{\mathrm{H}}_{\mathrm{Na}^+}\mathrm{d}\tilde{\mu}_{\mathrm{Na}^+} - \Gamma^{\mathrm{H}}_{\mathrm{Br}^-}\mathrm{d}\tilde{\mu}_{\mathrm{Br}^-}, \quad (1)$$

where s^{H}, v^{H}, and $\Gamma^{\mathrm{H}}_\alpha$ are respectively the surface excess entropy, volume, and surface density of ion α, which are defined with respect to the two dividing planes making the excess numbers of moles of air and water zero simultaneously [35, 41]. Introducing the electrochemical potential gives

$$\tilde{\mu}_\alpha = \mu_\alpha + z_\alpha F\phi, \quad (2)$$

where μ_α is the chemical potential of ion α, F is the Faraday constant, ϕ is the electrical potential, and z_α is the valence of ion α. The electroneutrality condition in the adsorbed film is

$$\Gamma^{\mathrm{H}}_{\mathrm{DTA}^+} + \Gamma^{\mathrm{H}}_{\mathrm{Na}^+} = \Gamma^{\mathrm{H}}_{\mathrm{Br}^-}, \quad (3)$$

which when inserted into Eq. 1 gives

$$\mathrm{d}\gamma = -\Gamma^{\mathrm{H}}_{\mathrm{DTA}^+}\mathrm{d}\mu_{\mathrm{DTA}^+} - \Gamma^{\mathrm{H}}_{\mathrm{Na}^+}\mathrm{d}\mu_{\mathrm{Na}^+} - \Gamma^{\mathrm{H}}_{\mathrm{Br}^-}\mathrm{d}\mu_{\mathrm{Br}^-}. \quad (4)$$

at a given T and p. Assuming that the bulk solution is ideally dilute as in the present case, Eq. 4 can be rewritten as a function of the molality of DTABr m_1 and NaBr m_2 as

$$\mathrm{d}\gamma = -RT\left[\Gamma^{\mathrm{H}}_{\mathrm{DTA}^+}\left(\frac{1}{m_1} + \frac{1}{m_1 + m_2}\right) + \Gamma^{\mathrm{H}}_{\mathrm{Na}^+}\left(\frac{1}{m_1 + m_2}\right)\right]_{T,p,m_2} \mathrm{d}m_1 - RT\left[\Gamma^{\mathrm{H}}_{\mathrm{DTA}^+}\left(\frac{1}{m_1 + m_2}\right) + \Gamma^{\mathrm{H}}_{\mathrm{Na}^+}\left(\frac{1}{m_2} + \frac{1}{m_1 + m_2}\right)\right]_{T,p,m_1} \mathrm{d}m_2. \quad (5)$$

The surface density of DTA^+ is evaluated from the dependence of γ on m_1 and m_2 with the use of

$$\Gamma^{\mathrm{H}}_{\mathrm{DTA}^+} = -\left[(1 + X_2)\left(\frac{\partial\gamma}{\partial \ln m_1}\right)_{T,p,m_2} - X_1\left(\frac{\partial\gamma}{\partial \ln m_2}\right)_{T,p,m_1}\right]/2RT, \quad (6)$$

where $X_2 = m_2/(m_1 + m_2)$. In the absence of added salt, Eq. 6 is reduced to

$$\Gamma^{\mathrm{H}}_{\mathrm{DTA}^+} = -\frac{m_1}{2RT}\left(\frac{\partial\gamma}{\partial m_1}\right)_{T,p}. \quad (7)$$

Surface quasi-elastic light scattering method

The SQELS apparatus was constructed based on that reported by Sakai et al. [42–44] as schematically illustrated in Fig. 1. The surface wave "ripplon" that was naturally excited by thermal motion of constituent molecules was detected and analyzed. The principles and details of the SQELS method have been described elsewhere [36, 42].

The incident ray of YAG ($Y_3Al_5O_{12}$) laser light (532 nm, 200 mW) was diffracted by the periodic surface displacement owing to the ripplon. The wavenumber k of the ripplon to be detected was determined by the scattering angle through the Bragg's condition (see Fig. 2):

$$k = K\sin\theta, \tag{8}$$

where K denotes the wavenumber of incident light and θ is the scattering angle. To gain sufficient signal intensity, we used the heterodyne method [42, 43]. A cell of the sample solutions was placed at the measurement point shown in Fig. 1 and covered with a thermostatic stage fitted with Peltier devices for temperature control. The difference of the frequencies between the incident and the scattered light was monitored in the form of a power spectrum (frequency domain) with the use of a spectrum analyzer. Note that the frequency of the reference light was shifted by 85 kHz by an acoustic optic (AO) modulator before it met the incident light, as shown in Fig. 1. This shift was introduced to remove the signal noise within the low frequency region. The apparatus set up here resulted in three peaks in the power spectrum; the central peak was related to the instruments and the two side peaks originated from the ripplon with k satisfying Eq. 8.

The main parts of the SQELS apparatus were as follows: YAG laser (Verdi-V5, Coherent), Acoustic Optic Modulator (TEM-85-2-532, Brimrose), Photomultiplier (C5331-11, Hamamatsu), and Spectrum Analyzer (MS2661C, Anritsu). The SQELS measurements were performed under atmospheric pressure for the respective systems as follows: (A), (C), and

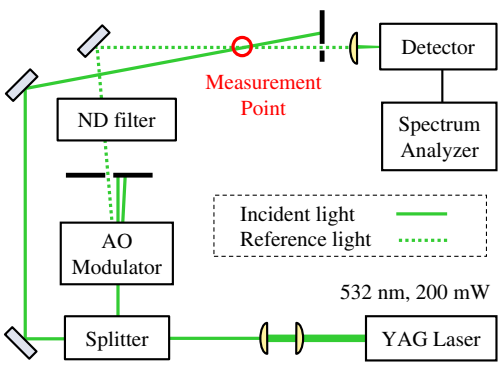

Fig. 1 Optical arrangement of the surface quasi-elastic light scattering (SQELS) device. Solid and dashed lines represent incident and reference lights, respectively

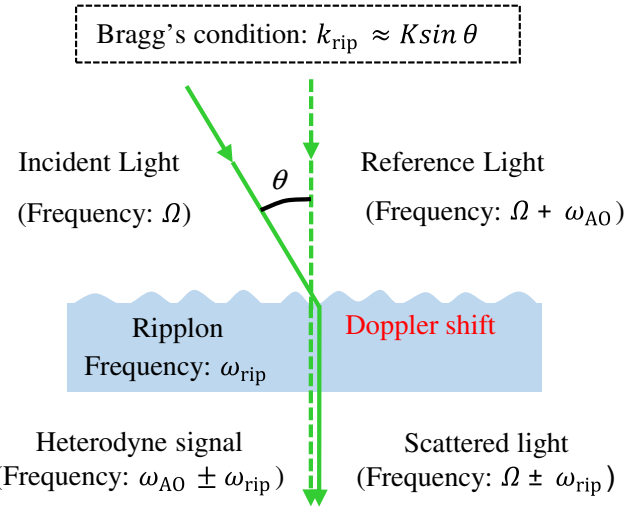

Fig. 2 Image of the light scattering from ripplon at the solution surface. Solid and dashed lines represent incident and reference lights, respectively

(D); at 298.15 K as a function of m_1, (B); at 298.15 and m_2/mmol kg^{-1} = 5 and 10 as a function of m_1.

Dispersion relation for air/water interface

A liquid surface is always fluctuating owing to thermal motion of its constituent molecules. The vertical displacement of a given point of the surface **r** at a time t can be written as [36]:

$$u(\mathbf{r},t) = \sum_{\mathbf{k}} u(\mathbf{k})\exp[i(\mathbf{k}\cdot\mathbf{r} - \omega(k)t)], \tag{9}$$

which is a sum of Fourier components at all wave vectors **k**. Taking account of that the surface tension γ is considered to be the main restoring force for surface transversal displacement and surface dilational viscoelasticity $\varepsilon^*(\omega)$ works against the surface longitudinal displacement, where ω is the real angular frequency of the surface wave. We obtain the following dispersion relation for an air/water interface in which both the density and viscosity of air are negligible [36, 45];

$$D(k,\omega) = L(\varepsilon^*;k,\omega) \times T(\gamma;k,\omega) + C(\eta,\rho) = 0, \tag{10}$$

where

$$L(\varepsilon^*;k,\omega) = \varepsilon^* k^2 + i\omega\eta(k+\mu), \tag{11}$$

$$T(\gamma;k,\omega) = \gamma k^2 + i\omega\eta(k+\mu) - \frac{\rho\omega^2}{k}, \tag{12}$$

and

$$C(\eta,\rho) = [i\omega\eta(k-\mu)]^2, \tag{13}$$

respectively. Here, $C(\eta, \rho)$ depends on density ρ and viscosity η of the aqueous phase and couples with the longitudinal quantity $L(\varepsilon^*; k, \omega)$ given by Eq. 11 and the transverse one

$T(\gamma; k, \omega)$ given by Eq. 12. Here, μ is the reciprocal of the penetration depth of the surface velocity field defined by

$$\mu^2 = k^2 + i\omega\rho/\eta. \tag{14}$$

In the classical dispersion relation, transversal waves are coupled with longitudinal ones and propagation characteristics of both waves depend on $\varepsilon^*(\omega)$, although the dependence of transversal wave is much weaker than that of longitudinal ones. It is known that the coupling between transversal and dilational waves becomes more effective at resonance for which the frequencies of two modes are close to each other, which generally occurs when the ratio $\varepsilon/\gamma \approx 0.16$ [23]. As shown later in Fig. 19, ε/γ changed from approximately 0.05 to 0.45, and good coupling [4] was observed at ε/γ values where the damping coefficient became a maximum.

Furthermore, $\varepsilon^*(\omega)$ is related to the variation of surface tension $\delta\gamma$ with surface area δA and is defined as follows:

$$\varepsilon^*(\omega) \equiv A\frac{\delta\gamma}{\delta A}. \tag{15}$$

Because of the dissipative effect within the adsorbed film, $\varepsilon^*(\omega)$ can be written as a complex number $\varepsilon^*(\omega) = \varepsilon(\omega) + i\omega\kappa(\omega)$, where $\varepsilon(\omega)$ and $\kappa(\omega)$ are the surface dilational elasticity and viscosity, respectively. The complex modulus $\varepsilon^*(\omega)$ contains two-dimensional isotropic compression (dilation), in-plane share and out-of-plane (transversal) share contributions. Because the order of the wavelength is sufficiently large compared with that of the amplitude of the surface wave of the surfactant aqueous solution, the out-of-plane share contribution is negligible [4, 36, 45]. Furthermore, the in-plane share contribution is also much smaller than the dilational one and negligible when the adsorbed film is fluid-like, such as a gaseous or an expanded film state.

For pure liquids without surface active substances, the surface dilational viscoelasticity term also disappears ($\varepsilon = \kappa = 0$) and when the complex frequency of the transversal wave is expressed as $\omega + i\Gamma$, we obtain two limiting solutions of the dispersion equation at a wavenumber of k; one is Kelvin's law for the frequency

$$\omega^2 \approx \frac{\gamma}{\rho}k^3. \tag{16}$$

and the other is Stokes' law for the damping caused by the viscous friction with the bulk liquid:

$$\Gamma \approx \frac{2\eta}{\rho}k^2. \tag{17}$$

Surface rheological fitting analysis

The spectrum obtained from SQELS method was compared with the theoretical power spectrum equation of Kramer [46] for transversal wave in the presence of air given by

$$P_T(k,\omega) = \frac{k_B T}{\pi\omega}\mathrm{Im}\left[\frac{L(\varepsilon^*; k, \omega)}{D(k,\omega)}\right], \tag{18}$$

where k_B is the Boltzmann constant. Equation 18 corresponds to the inverse Fourier transform of the auto correlation function of the surface wave. Because side peaks originating in a ripplon are generally broadened owing to instrumental considerations in the SQELS technique [12], some calibration processes are required. In our case, we determined the wavenumber of the ripplon k_{rip} and the instrumental resolution β on the basis of the SQELS results and the reference values of pure water. The spectrum from a pure water surface should be free from surface viscoelasticity, and thus, instrumental parameters such as k_{rip} and β can be determined. The reference values of fitting parameters of pure water at $T = 298.15$ K were $\rho = 997.047$ kg m^{-3}, $\eta = 0.89$ mPa · s, and $\gamma = 71.96$ mN m^{-1}, respectively. The SQELS spectrum from pure water provided a larger width than that theoretically calculated from Eq. 17 and it was fitted by k_{rip} and β with $\varepsilon = \kappa = 0$ in Eq. 18. Hence, the frequency ω and damping coefficient Γ simultaneously satisfied Kelvin's law of Eq. 16 and Stokes' law of Eq. 17, respectively, for the various wavenumbers k_{rip} from 70 to 320 cm^{-1}.

Because the instrumental resolution was dependent on the wavenumber, the uncertainty of the wavenumber δk_{rip} was taken into account by the following equations [47]:

$$P_{exp}(k,\omega) = A\int\rho\left(k, k'\right)P_T\left(k', \omega\right)\mathrm{d}k', \tag{19}$$

and

$$\rho\left(k'-k\right) = \frac{1}{\sqrt{\pi}\beta}\exp\left[-\frac{\left(k'-k\right)^2}{\beta^2}\right]. \tag{20}$$

where A is an arbitrary constant and β is the uncertainty of wavenumber of ripplon δk_{rip}. Equations 19 and 20 imply that the experimentally obtained spectrum $P_{exp}(k, \omega)$ is a convolution of a theoretical function and a Gaussian function of wavenumber.

In principle, the surface rheological fitting analysis by Eqs. 10 to 14 and Eqs. 18 to 20 yields the surface dilational viscoelasticity $\varepsilon^*(\omega)$ of the surfactant aqueous solutions. However, to determine the surface dilational viscoelasticity more accurately, the equilibrium surface tension γ of the aqueous solutions measured separately from the SQELS studies was used as a fixed parameter in Eq. 18. Thus, the surface dilational elasticity ε and viscosity κ were determined as the main and sub fitting parameters in Eq. 18, respectively. Furthermore, Cicuta et al. [12] indicated that this treatment provides a general justification for the correct recent practice of SQELS experiments, which is very different from earlier

ones where the four quantities of surface dilational elasticity, surface dilational viscosity, transverse share elasticity (surface tension), and transverse share viscosity were usually chosen as physical parameters [20, 48, 49]. The surface rheological fitting analysis was performed by a fitting program coded in FORTRAN that was constructed with support from Ohmasa et al. [47]. The values of ε and κ were respectively determined to be in the range of $0 \le \varepsilon(\omega) \le 100$ mN m^{-1} and $-1000 \le \kappa(\omega) \le 1000$ nNs m^{-1}. This is because the shape of the power spectrum of scattered light tends to become independent of the surface dilational viscoelasticity as it becomes larger [12].

The SQELS measurements were performed at fixed wavenumbers for all surfactant solutions: $k_{\mathrm{rip}} \approx 200$ cm^{-1} and $\delta k_{\mathrm{rip}} \approx 20$ cm^{-1}, which were determined from the SQELS measurements of pure water.

Phenomenological fitting analysis

From the phenomenological fitting analysis of the SQELS spectrum, both the angular frequency ω and damping coefficient Γ, $\omega + i\Gamma$, of ripplons were evaluated. In our experimental setup, the central peak and two side peaks could be accurately described by a Gaussian function and by a Voigt function, respectively. The experimentally obtained spectrum $P_{\mathrm{exp}}(\omega)$ is a convolution of Lorentzian function and Gaussian function of frequency given by

$$P_{\mathrm{exp}}(\omega) = A\int \rho\left(\omega - \omega'\right) P_P\left(k, \omega'\right) \mathrm{d}\omega', \tag{21}$$

where $P_P(k, \omega')$ is the phenomenological power spectrum equation:

$$P_P\left(k, \omega'\right) = \Gamma\left\{\frac{1}{\left[\left(\omega' - \omega_{\mathrm{AO}}\right) + \omega_{\mathrm{rip}}\right]^2 + \Gamma^2} + \frac{1}{\left[\left(\omega' - \omega_{\mathrm{AO}}\right) - \omega_{\mathrm{rip}}\right]^2 + \Gamma^2}\right\}, \tag{22}$$

and

$$\rho\left(\omega - \omega'\right) = \mathrm{F.T.}\left[\exp\left\{-\frac{\left(\left(\omega - \omega_{\mathrm{AO}}\right) - \omega'\right)^2}{2\beta^2}\right\}\right], \tag{23}$$

where ω_{AO} is the frequency shift introduced by the AO modulator and F.T. means Fourier transformation. In Eq. 23, the resolution β was the value of $\delta\omega_{\mathrm{rip}}$ calculated using δk_{rip} by

$$\delta\omega_{\mathrm{rip}} = \frac{3}{2}\sqrt{\frac{\gamma}{\rho}} k_{\mathrm{rip}}^{\frac{1}{2}} \delta k_{\mathrm{rip}}. \tag{24}$$

Equation 24 is derived from Kelvin's law given by Eq. 16.

Results and discussion

SQELS and ECW studies of short-chain phospholipid mixtures (DC_8PC+DC_6PC)

The aqueous lipid solutions were used to form monolayers because both lipids have short chains and are thus soluble in water. Their surface tension was measured as a function of the total concentration of the two lipids at fixed mixing ratios and the surface concentrations were evaluated by thermodynamic equations as described in our recent paper [24]. Figure 3a shows the SQELS spectrum at given surface mole fractions of DC_8PC, defined by $X_2^{\mathrm{H}} = \Gamma_{\mathrm{DC8PC}}^{\mathrm{H}} / \left(\Gamma_{\mathrm{DC6PC}}^{\mathrm{H}} + \Gamma_{\mathrm{DC8PC}}^{\mathrm{H}}\right)$ at 35 mNm^{-1}. As mentioned in the experimental section, the angle of the incident light was fixed and accordingly the wavenumber of the detected transversal wave was fixed, which means that the ripplon frequency is proportional to the ripplon wave velocity. Figure 3b shows that the ripplon (angular) frequency $\omega_{\mathrm{rip}} = 2\pi f$ was approximately 250 kHz and decreased by 35% compared with that of pure water surface owing to the adsorption of the lipid mixtures at approximately 2.8 μmol m^{-2} and $\gamma =$ 35 mNm^{-1} [24]. Conversely, the damping coefficient of the adsorbed film was almost the same as that of pure water surface (dotted line), as shown in Fig. 3c.

The dilational elasticity at approximately 250 kHz from the SQELS is plotted against X_2^{H} together with that at 0.2 kHz from the ECW in Fig. 4, where we note the following points. The former seems to pass through a very shallow minimum; however, the latter evidently passes through a maximum [24]. There exists a clear difference in the dilatational elasticity between the longer and shorter chain lipids at 0.2 kHz; however, this difference almost disappears at approximately 250 kHz. Moreover, the maximum, which appeared at 0.2 kHz was not observed at 250 kHz. The van der Waals interactions among the hydrophobic chains in the oriented adsorbed layer were stronger for DC_8PC than for DC_6PC and a staggered structure of the adsorbed film was indicated by examination of the minimum of the excess Gibbs energy of adsorption $g^{\mathrm{H,\,E}}$ (dashed curve in Fig. 4) around $X_2^{\mathrm{H}} = 0.3$ [24]. Hence, molecular interactions in the adsorbed films clearly influenced the relaxation process on the order of several milliseconds (ECW); however, these interactions were less influential on the order of several hundreds of microseconds (SQELS).

We next examined whether the relaxation processes owing to the staggered structure formation was of the order of milliseconds or not. The dilational viscoelasticity was determined as a function of frequency by ECW. The storage and loss modulus, ε and $\omega\kappa$, are plotted against the frequency at four surface mole fractions in Fig. 5a. The storage modulus increased with increasing frequency; however, the loss modulus showed a maximum from 150 to 300 Hz. When the frequency

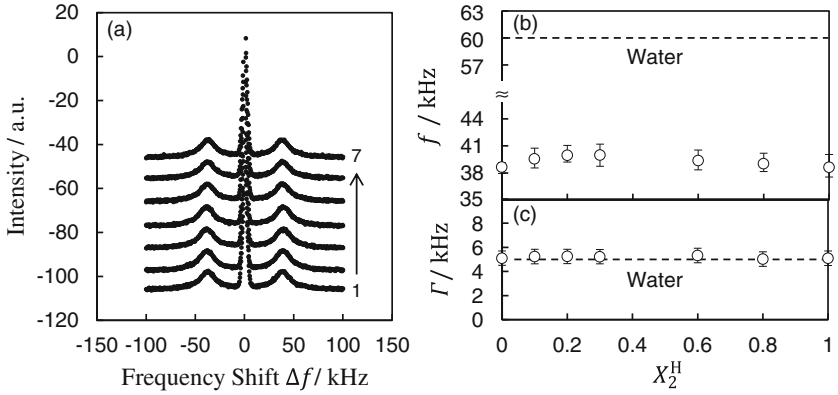

Fig. 3 SQELS results of the DC_6PC-DC_8PC mixtures at a surface tension of 35 mN m^{-1}. **a** SQELS spectra at X_2^H = (1) 0, (2) 0.1, (3) 0.2, (4) 0.3, (5) 0.6, (6) 0.8, and (7) 1. **b** ripplon frequency f and **c** damping coefficient Γ plotted against surface mole fraction of DC_8PC X_2^H

of surface deformation is comparable to the time scale of the dynamic process, the storage modulus curve has an inflection and the loss modulus has a maximum around the characteristic frequencies, as schematically illustrated in Fig. 5b [3, 4]. Therefore, we confirmed that the characteristic frequencies for the mixed adsorbed films of the DC_8PC+DC_6PC system likely lie in the range from 150 to 300 Hz. At 200 Hz, i.e., the maximum of the storage modulus, which appears at $X_2^H = 0.5$ in Fig. 4, is between 150 and 300 Hz. This surface mole fraction is closed to that at the minimum excess Gibbs energy attributable to the staggered structure of the adsorbed film. We concluded that the characteristic frequency of the staggered structure formation is of the order of a few hundred Hz and the characteristic time scale for the relaxation of the staggered structure is of the order of milliseconds. Ravera et al. demonstrated that the storage modulus owing to diffusion of molecules between the bulk and surface shows an inflection and the corresponding loss modulus shows a maximum at a very low frequency of the order of 10^{-2} Hz [3]. Conversely, relaxations such as surfactant reorientation and aggregation in the surface have much higher characteristic frequencies. For example, for adsorption of tetraethylene glycol monodecyl ether ($C_{10}E_4$), the characteristic frequency for diffusion was approximately 0.4 Hz, while that for surfactant reorientation was suggested to be 800 Hz. Judging from these observations, the staggered structure formation was minimally influential on the dilational elasticity at 250 kHz, which is in accord with our observations in Fig. 4 that the dilational elasticity does not change greatly with the surface composition at 250 kHz.

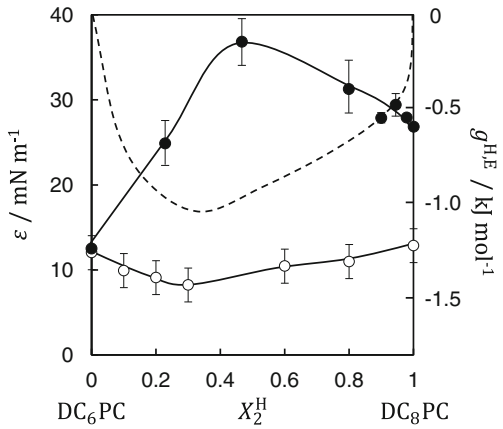

Fig. 4 Comparison between the results of SQELS and ECW for the DC_6PC-DC_8PC mixtures. Dilational elasticity ε vs. X_2^H at surface tension of 35 mN m^{-1}. f (kHz) = 40 (SQELS, ○) and 0.2 (ECW, ●). Dashed curve represents excess Gibbs energy of adsorption $g^{H,E}$

Diffusion of small chemical species might show a much faster relaxation process, compared with diffusion of surfactant molecules between the bulk and surface, and surfactant reorientation and aggregation at the surface. Hence, counterions of ionic surfactants are appropriate candidates because of their typically small size. Furthermore, these molecules move back and forth between the Stern layer and diffuse layer regions in the electrical double layer. Another candidate is water molecules because these undergo cycles of hydration and dehydration around the hydrophilic groups of surfactants. For this purpose, nonionic surfactants with ethylene oxide units are appropriate. On the basis of these ideas, the SQELS method was applied to cationic surfactants with different counter ions and nonionic ones with ethylene oxide units.

SQELS studies of cationic surfactants with different counterions

Now, let us show the dilational elasticity of aqueous solutions of (A) DTABr, (B) DTABr in the presence of NaBr, and (C) $DTABF_4$ and DTA_2SO_4. Studies on (A) and (B) provide information about what kind of relaxation processes influence dilational elasticity at high frequencies of a few hundred kHz. The Lucassen and van den Temple (LT) and modified LT (MLT) models for the dilational viscoelasticity [17, 37–39] are introduced and used to investigate the kind of information that can be derived from the models. Studies on system (C) offer information about whether the degree of counter ion binding to the surfactant ion is influential or not on dilational viscoelasticity, because BF_4^- is more hydrophobic than Br^- and SO_4^{2-} is divalent. Furthermore, the distribution of Br^- in the electrical double layer of the adsorbed monolayers has

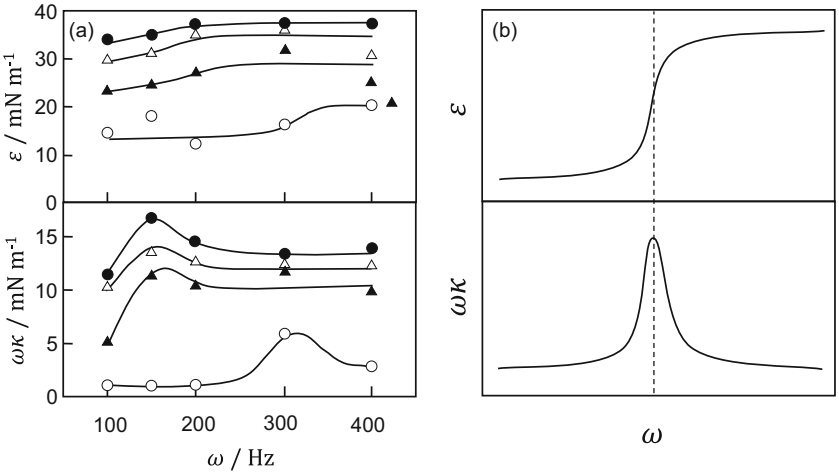

Fig. 5 Frequency dependency of dilational elasticity (storage modulus) ε and loss modulus. **a** experimental results of the DC_6PC-DC_8PC mixtures at X_2^H = 0 (○), 0.2 (●), 0.5 (△), and 1 (▲). **b** schematic curves [Ref. 4]

been investigated by means of the total reflection XAFS method in our studies [33, 34].

Dodecyltrimethylammonium bromide

The surface tension γ vs surfactant concentration m_1 curves are displayed up to the concentrations just below the critical micelle concentrations in Fig. 6, and the corresponding curves of the surface density of surfactant ions $\Gamma^H_{DTA^+}$ are given in Fig. 7. Break points on the surface tension curve and corresponding discontinuous changes on the surface density curve observed in the absence of NaBr are often found for various kinds of surfactants and have been attributed to a phase transition of adsorbed films from a gaseous to an expanded state [25, 26].

The SQELS spectra of DTABr at various concentrations are shown in Fig. 8. All the spectra were symmetrical with respect to the top of the central peak at a frequency shift $\Delta f = 0$ and their shape changed regularly with surfactant concentration. The angular wave frequency of the side peaks ω and the damping coefficients Γ of ripplon were evaluated by phenomenological fitting with Eq. 22 and the ratio ω/ω_{water} and Γ/Γ_{water} are plotted against concentration together with those in the presence of NaBr in Fig. 9. The value of ω/ω_{water} clearly changed continuously but showed a break at a concentration (m_1^{br}), which almost coincided with the phase transition concentration determined from the surface tension measurements in the absence of NaBr. In the presence of NaBr, although a break was not observed on the surface tension curves, the ω/ω_{water} curves showed a break, which suggests that the surface wave properties were more influenced by the phase transition compared with surface tension [50]. Furthermore, Γ/Γ_{water} values pass through a maximum at a concentration m_1^{mx} slightly above m_1^{br}; the combinations of $\left(m_1^{br}/\text{mmol kg}^{-1}, m_1^{mx}/\text{mmol kg}^{-1}\right)$ are roughly (2.0, 2.5), (0.75, 1.0), (0.30, 0.50) for DTABr, DTABr+NaBr (m_2/mmol kg^{-1} = 5) and DTABr + NaBr (m_2/mmol kg^{-1} = 10), respectively.

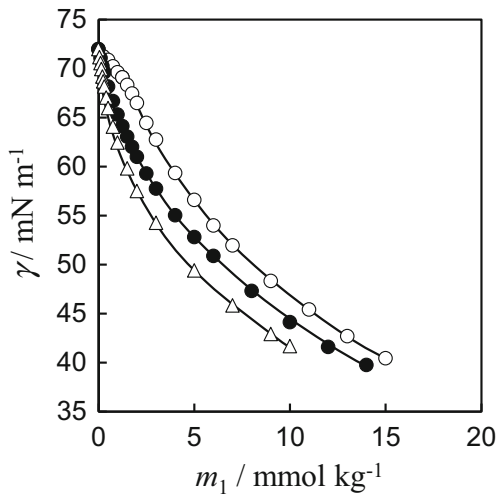

Fig. 6 Surface tension γ vs. molality m_1 curves of the DTABr-NaBr mixtures at m_2 (mmol kg^{-1}) = 0 (○), 5 (●), and 10 (△)

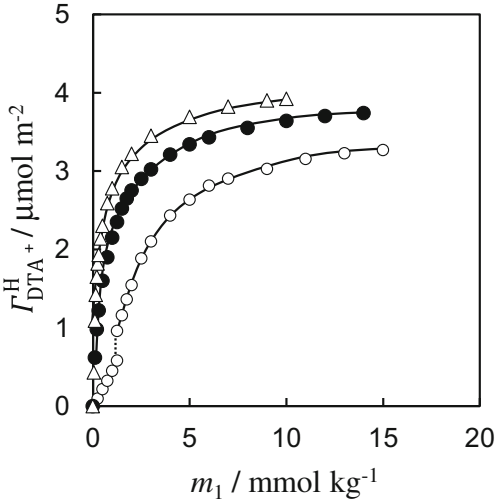

Fig. 7 Surface density $\Gamma^H_{DTA^+}$ vs. molality m_1 curves of the DTABr-NaBr mixtures at m_2 (mmol kg^{-1}) = 0 (○), 5 (●), and 10 (△)

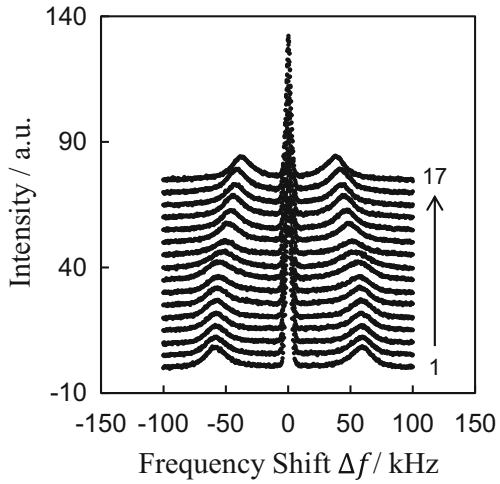

Fig. 8 SQELS spectra of DTABr at m_1 (mmol kg^{-1}) = (1) 0.25, (2) 0.5, (3) 0.75, (4) 1.0, (5)1.25, (6) 1.5, (7) 1.5, (8) 1.75, (9) 2.0, (10) 2.5, (11) 3.0, (12) 5.0, (13) 7.0, (14) 9.0, (15) 11, (16) 13, and (17) 15

Although it is clear from the experiments that the breaks on the ω/ω_{water} curves plotted against surfactant concentration or temperature are attributable to phase transitions of the interfacial films, it remains unclear whether the maximum of Γ/Γ_{water} stems from such a phase transition or from coupling between the in-plane (dilational and shear) and out-of-plane (capillary) waves. Kizling et al. studied the viscoelastic properties of adsorbed monolayers of dodecylammonium chloride and identified such a break on the ω curve and a maximum on the Γ curve just above m_1^{br} [51], which was essentially the same as our observations for DTABr. They claimed that ω is strongly affected by changes of surface tension and although there is a very small discontinuous change of Γ at the phase transition point, the peak of Γ is obviously rather closely related to the phase transition. Monroy et al. also reported capillary waves of the dodecylammonium chloride solution that the change of slope observed for the ω vs concentration curves followed the variation of equilibrium surface tension; thus, the break on the ω curve corresponds to the surface phase transition [23]. Furthermore, they demonstrated that two maxima appear on the Γ curve at very low concentration and at a concentration slightly above m_1^{br} corresponding to resonance between the capillary and dilational modes [23]. With respect to the Langmuir monolayer of hydrophobin, Aumaitre et al. showed that ω decreases with increasing surface concentration and forms a plateau between surface concentrations of 1.6 and 1.8 mg m^{-2}. This finding could indicate the coexistence of condensed and liquid domains, whereas the surface pressure remained null up to around 2.2 mg m^{-2} [50]. On the basis of these findings, they emphasized that a decrease in ω does not necessarily indicate an increase of surface pressure but could also be a signature of an increase in the dilational modulus. Furthermore, they described that the damping coefficient Γ presents a peak at a concentration of the coexistence region, which corresponds to the maximum coupling between the in-plane and out-of-plane waves, that is, $(\varepsilon/\gamma) \sim 0.16$ [20, 23, 36, 52, 53]. Munoz et al. observed a break of ω and Γ, rather than a maximum at the temperature of the 2D liquid-solid phase transition for 1-dodecanol monolayers [54]. Considering our observation that the concentrations m_1^{mx} are different from those at the phase transition m_1^{br} and the dilational elasticity to surface tension ratio (ε/γ) is 0.15–0.16 for DTABr at m_1^{mx} (see Fig. 19), the maximum of Γ can be attributed to coupling of the in-plane and out-of-plane waves [36].

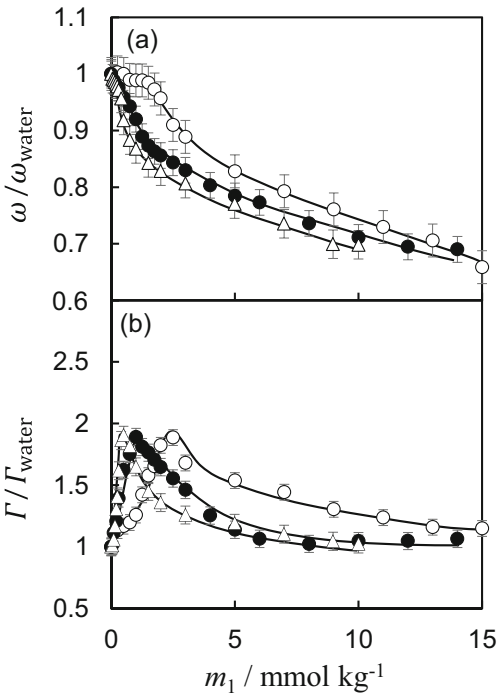

Fig. 9 (a) Ripplon frequency ω/ω_{water} and (**b**) damping coefficient Γ/Γ_{water} from phenomenological fitting of the DTABr-NaBr mixtures plotted against molality m_1 at m_2 (mmol kg^{-1}) = 0 (○), 5 (●), and 10 (△)

The surface dilational viscoelasticity $\varepsilon^*(\omega) = \varepsilon(\omega) + i\omega\kappa(\omega)$ was calculated by surface rheological fitting analysis with Eq. 18. Figure 10a shows the dilational elasticity $\varepsilon(\omega)$ and the ripplon

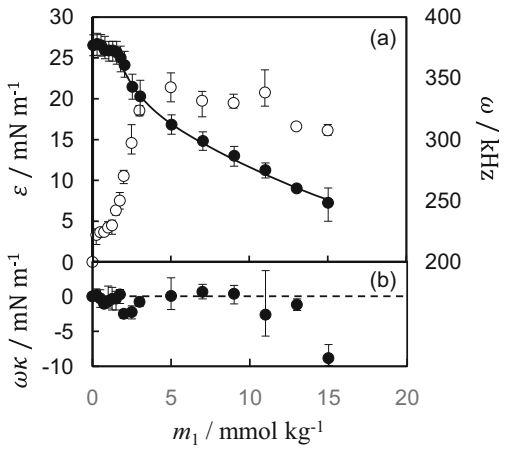

Fig. 10 Dilational viscoelastic properties of DTABr. (a) dilational elasticity (storage modulus) ε (○), ripplon frequency ω (●), and (b) dilational loss modulus $\omega\kappa$ plotted against molality m_1

angular frequency ω and Fig. 10b shows the dilational loss modulus $\omega\kappa(\omega)$. The value of $\varepsilon(\omega)$ increased from zero for pure water surface to be in the range of 4–5 mN m^{-1} and became steady in the gaseous state. In the expanded state, the value initially increased steeply in response to a steep increase in the surface density, then passed through a maximum and decreased gradually despite the continuous increase in surface density. The absolute value of $\omega\kappa(\omega)$ was 0–10 mN m^{-1} and its contribution to $\varepsilon^*(\omega)$ was non-negligible compared with the elasticity $\varepsilon(\omega)$. Because the dilational viscosity has unrealistic negative values, which have been discussed from consideration of the adsorption barrier and applicability of the dispersion equation generally employed [20, 23], the dilational elasticity will be the main focus of this paper.

The change of dilational elasticity with bulk concentration has been examined in terms of diffusion of surfactant molecules between the monolayer and the underlying aqueous phase with the use of the Lucassen and van den Tempel (LT) model [37, 55, 56]. Molecules in the adsorbed films on the aqueous surfactant solutions are dissolved or adsorbed upon compression or expansion to restore the equilibrium surface concentration. Because the shear coefficients are reasonably assumed to be negligible compared with the dilational coefficients, the complex dilational viscoelasticity ε^* is defined as the fluctuation of local surface tension γ_l accompanied by a change of surface area A, described by

$$\varepsilon^* = A\left(\frac{\partial\gamma_l}{\partial A}\right) = \left(\frac{\partial\gamma_l}{\partial \ln A}\right). \tag{25}$$

When any relaxation process is either much faster or much slower than the time scale of experiments $\tau_{exp} = \omega^{-1}$ (in the SQELS study, this is the time scale of detected ripplon), the variation of surface tension accompanied by the surface expansion and contraction is instantaneous, and thus, the surfaces behave as if they are purely elastic. Let us designate $\varepsilon^*(\omega) = \varepsilon(\omega) = \varepsilon_0$ in such purely elastic cases.

Purely elastic cases are realized when two conditions are fulfilled. The first condition is that reorientation of constituent molecules in the monolayer is completed on a time scale of the order of $\tau_{exp} = \omega^{-1}$, and thus, the equilibrium between the local surface tension and the surface density Γ should be very quickly established. The other is that diffusional exchange between the surface and bulk is negligible, and thus, the total amount of adsorbed molecules does not change on a time scale of the order of $\tau_{exp} = \omega^{-1}$, i.e., even a soluble monolayer behaves as if it is an insoluble one with respect to this time scale. Therefore, ε_0 can be written as

$$\varepsilon_0 = \left(\frac{\partial\gamma^{eq}}{\partial \ln A^{eq}}\right) = -\left(\frac{\partial\gamma^{eq}}{\partial \ln \Gamma^{eq}}\right) \tag{26}$$

and evaluated using the equilibrium relation between the surface tension vs surface density Γ^{eq} (= Γ_1^H in this paper, Γ_1^H denotes $\Gamma_{DTA^+}^H$ or Γ_{C10E5}^H in the following discussion). The variable ε_0 is commonly known as the Gibbs elasticity. There is a well-known procedure based on the Frumkin equation of state for calculating ε_0 and it often satisfactorily describes the variation of surface pressure with the bulk concentration. When the Frumkin equation was applied to the DTAB system, Stenvot et al. reported ε_0 values of 280 mNm^{-1} at 10 mM [18], which is comparable to the highest values for DTAB near CMC in our calculations, as shown later in Fig. 11. Now, let us rewrite Eq. 25 as

$$\varepsilon^* = \left(\frac{\partial\gamma_l}{\partial \ln\Gamma_l}\right)\left(\frac{\partial \ln\Gamma_l}{\partial \ln A}\right), \tag{27}$$

and assume that the equilibrium between the local surface tension and the surface density Γ is rapidly established as $\left(\frac{\partial\gamma_l}{\partial \ln\Gamma_l}\right) \approx \left(\frac{\partial\gamma_l}{\partial \ln\Gamma_l}\right)$. Whether this assumption is appropriate or not is another important issue, particularly for high-frequency experiments like SQELS. With this assumption, we obtain

$$\varepsilon^* = -\varepsilon_0\left(\frac{\partial \ln\Gamma_l}{\partial \ln A}\right). \tag{28}$$

When the reorientation processes of constituent molecules in the monolayer is completed within a time scale of the order of ω^{-1}, barriers against both adsorption and desorption are absent, and the molecular exchange is controlled solely by diffusion between the subsurface and bulk solution. The factor $\left(\frac{\partial \ln\Gamma_l}{\partial \ln A}\right)$ can be derived from the first and second laws of Fick to give

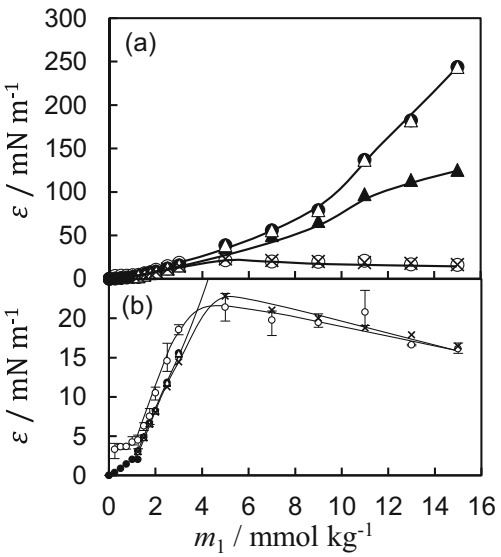

Fig. 11 (a) Comparisons among the dilational elasticities obtained from experiments and models for DTABr and (b) enlarged view. ε from experiments (○), Gibbs elasticity ε_0 (●), LT model ε_{LT} (▲), MLT model ε_{MLT} (△), effective LT model $\varepsilon_{LT,\,eff}$ (×)

the dilational elasticity ε_{LT} and viscosity κ_{LT} from the LT model as

$$\varepsilon_{LT} = \varepsilon_0 \frac{1+\tau}{1+2\tau+2\tau^2}, \tag{29}$$

and

$$\omega\kappa_{LT} = \varepsilon_0 \frac{1}{1+2\tau+2\tau^2}. \tag{30}$$

Here, τ is a dimensionless parameter given by

$$\tau = \sqrt{D/2\omega}\left(\mathrm{d}m_1/\mathrm{d}\Gamma_1^{\mathrm{H}}\right), \tag{31}$$

where D represents the diffusion coefficient of surfactant in the bulk solution [37]. This is the equation of the LT model. Because the characteristic frequency of diffusion ω_{dif} and thus the characteristic diffusion time τ_{dif} are given by [23]

$$\omega_{dif} = {\tau_{dif}}^{-1} = (D/2)\left(\mathrm{d}m_1/\mathrm{d}\Gamma_1^{\mathrm{H}}\right)^2, \tag{32}$$

where τ expresses the ratio of the time scale of the relevant experiment ω^{-1} to that of the diffusion of surfactant molecule ${\omega_{dif}}^{-1}$ as

$$\tau = \sqrt{\omega_{dif}/\omega} = \sqrt{\tau_{exp}/\tau_{dif}}. \tag{33}$$

Furthermore, when an adsorption barrier is taken into account in the LT model (the modified LT model, MLT), Eq. 29 is converted to

$$\varepsilon_{MLT} = \varepsilon_0 \frac{1+(1+2\alpha)\tau+2\alpha^2\tau^2}{1+2(1+\alpha)\tau+2(1+\alpha^2)\tau^2}, \tag{34}$$

where $\alpha = \omega/\left(k_d/\Gamma_1^{\mathrm{H}}\right)$ and k_d is the rate constant of desorption in the presence of adsorption-desorption barriers [17].

Summarizing the limiting properties of ε_{LT} and ε_{MLT}, we obtain

Case 1: Diffusion requires a much longer time than the experiment time scale ($\tau_{dif} \gg \tau_{exp}$) or the experiment frequency is much higher than diffusion ($\omega \gg \omega_{dif}$): $\tau \to 0$, $\varepsilon_{LT} \to \varepsilon_0$

Case 2: The opposite of case 1, ($\tau_{dif} \ll \tau_{exp}$) or ($\omega \ll \omega_{dif}$):

$\tau \to$ large, $\varepsilon_{LT} \to 0$

Case 3: The adsorption barrier is very low $\left[\left(k_d/\Gamma_1^{\mathrm{H}}\right) \gg \omega\right]$:

$(\alpha) \to 0$, $\varepsilon_{MLT} \to \varepsilon_{LT}$

Case 4: The experimental frequency is very high $\left[\left(k_d/\Gamma_1^{\mathrm{H}}\right) \ll \omega\right]$:

$\alpha \to$ large, $\varepsilon_{MLT} \to \varepsilon_0$.

Now, let us examine whether the LT and MLT models can describe the dilational elasticity given in Fig. 10a. Figure 11 shows the ε and ε_0 vs concentration curves, where ε_0 was evaluated from the equilibrium surface pressure vs mean area curve. Because ε is slightly larger than ε_0 in the low concentration range (see Fig. 11b), neither ε_{LT} nor ε_{MLT} can trace ε entirely in principle. Nevertheless, we tried to apply Eqs. 29 and 34 to the experimental ε vs concentration data using the diffusion coefficients of the surfactant in the aqueous phase $D = 6 \times 10^{-10}\mathrm{m}^2\ \mathrm{s}^{-1}$ and the rate constant of desorption $k_d = 1.68 \times 10^{-4}\mathrm{mol\ m}^{-2}\ \mathrm{s}^{-1}$ [57–59]. The results are also given in Fig. 11; ε_{LT} was lower than ε_0 and became close to ε. Thus, there may be some contributions from surfactant ion diffusion from the bulk to the subsurface on the dilational elastic properties. However, ε_{LT} remained much higher than ε and could not follow the ε values even in the high concentration region, where the effects of diffusion are expected to be more influential. Furthermore, the ε_{MLT} values were almost equal to ε_0 and the presence of a barrier to the adsorption-desorption process of surfactant ions has little influence on the dilational elastic behavior (i.e., case 4). These findings indicate that at the higher ripplon frequency detected by the present SQELS method, that is, ω of 200–400 kHz (see Fig. 10), the relaxation processes that influence the dilational properties are neither diffusion of surfactant from the bulk phase to the subsurface nor an adsorption-desorption of surfactant ions between the adsorbed layer and subsurface. The actual relaxation processes occur at the interfacial region.

Because the chemical structure of surfactants and counterions is very simple, relaxation caused by conformational changes is unlikely. Furthermore, the lateral diffusion of surfactant molecules in a monolayer is known to be very slow, e.g., the diffusion coefficient is of the order of $10^{-11}\ \mathrm{m}^2\ \mathrm{s}^{-1}$ [1]. Thus, let us assume some other possible diffusion processes are related to the counterions with an effective diffusion constant D_E within the scheme of the LT model as

$$\varepsilon_{LT,eff} = \varepsilon_0 \frac{1+\tau_{eff}}{1+2\tau_{eff}+2{\tau_{eff}}^2}, \tag{35}$$

where

$$\tau_{eff} = \sqrt{\omega_{dif,eff}/\omega}, \tag{36}$$

and

$$\omega_{\mathrm{dif,eff}} = \tau_{\mathrm{dif.eff}}{}^{-1} = (D_{\mathrm{E}}/2)\left(\mathrm{d}m_1/\mathrm{d}\Gamma_1^{\mathrm{H}}\right)^2. \quad (37)$$

In this case, D_{E} is likely related to the diffusion processes of chemical species other than surfactant ions. These processes do not occur between the subsurface and bulk, but rather within the interfacial region. It is clear in Fig. 11 that the value of $\varepsilon_{\mathrm{LT,\ eff}}$ traces the experimental value of ε more closely than those of ε_0, $\varepsilon_{\mathrm{LT}}$ and $\varepsilon_{\mathrm{MLT}}$. However, there is a small deviation of $\varepsilon_{\mathrm{LT,\ eff}}$ from ε at lower concentrations. The D_{E} value of the best fit was 7.12×10^{-8} m^2 s^{-1}. It should be noted that this value is almost hundred times as high as D and comparatively close to the diffusion coefficient of bromide ions in aqueous solution 2.1×10^{-9} m^2 s^{-1} and water 2.30×10^{-9} m^2 s^{-1} [60].

In our previous studies on the solvation structure of bromide ions in adsorbed DTABr monolayers by means of the total reflection XAFS, we demonstrated that there are essentially two kinds of bromide ions; ions of one group are hydrated by six water molecules (designated as free-Br), which exist in the diffuse layer. The second group includes those that are dehydrated by approximately three water molecules from free-Br and form ion pairs with cationic head groups of the surfactant monolayer (designated as bound-Br) existing in the Stern layer. In addition, the ratio of bound-Br defined by χ = bound-Br/(free-Br + bound-Br) can be approximated by $\chi = 0.27\Gamma^{\mathrm{H}}_{\mathrm{DTA}^+}$ in the expanded film of DTABr for pure DTABr and also in the presence of added NaBr of 10 mmol kg^{-1} [61]. The lateral diffusion of surfactant molecules in the monolayer is very slow compared with the time scale of detecting ripplons of ω^{-1} [1]. Thus, the surface dilation by capillary waves continually produces regions with a higher local surface density (HLSD) of a lower local surface tension and regions with a lower surface density (LLSD) of a higher local surface tension, relative to the average surface density $\Gamma^{\mathrm{H}}_{\mathrm{DTA}^+}$. The counter ions in the LLSD regions prefer to migrate into the diffuse layer; those in the diffuse layer diffuse onto the surfactant cationic head groups in the HLSD region. This effect may enhance the diffusion of counterions in the electrical double layer and raise the D_{E} value from the usual value of 2.1×10^{-9} m^2 s^{-1} to the observed value of 7.12×10^{-8} m^2 s^{-1}. Therefore, it is likely that a kind of Marangoni effect is taking place in the interfacial region on a very short time scale, which is different from the two typical types of mechanism related to the Marangoni effect (namely, adsorption/desorption of surfactants from/to bulk solution and the lateral diffusion within the adsorbed layer).

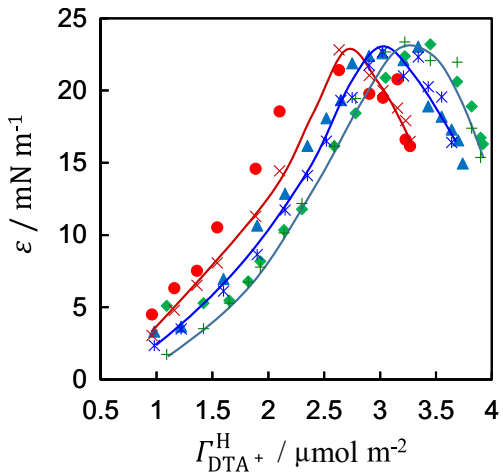

Fig. 12 Dilational elasticity vs. surface density $\Gamma^{\mathrm{H}}_{\mathrm{DTA}^+}$ of DTABr. ε at m_2 (mmol kg^{-1}) = 0 (●), 5 (▲), and 10 (■). $\varepsilon_{\mathrm{LT,\ eff}}$ at m_2 (mmol kg^{-1}) = 0 (×), 5 (*), and 10 (+). Solid curves represent a guide to the eyes for $\varepsilon_{\mathrm{LT,\ eff}}$

Let us investigate whether the addition of inorganic electrolyte influences the dilational elasticity and the diffusion coefficient. The dilational elasticity ε and the best fit of $\varepsilon_{\mathrm{LT,\ eff}}$ using Eq. 35 are plotted against the surface density in Fig. 12. Some distinctive features should be noted. First, the D_{E} values for the best fit of $\varepsilon_{\mathrm{LT,\ eff}}$ were 7.12×10^{-8} m^2 s^{-1}, 1.06×10^{-8} m^2 s^{-1}, and 1.99×10^{-8} m^2 s^{-1} at m_2/mmol kg^{-1} = 0, 5, and 10, respectively. Second, the ε vs $\Gamma^{\mathrm{H}}_{\mathrm{DTA}^+}$ curve shifted to the right as the NaBr concentration was increased. Third, the maximum values of ε are very close to each other but the surface density at the maximum ε, $\Gamma^{\mathrm{H,max}}_{\mathrm{DTA}^+}$, increases as m_2 increases.

Figure 12 also shows that $\varepsilon_{\mathrm{LT,\ eff}}$ fits ε very well at m_2/mmol kg^{-1} = 10 but the deviation of $\varepsilon_{\mathrm{LT,\ eff}}$ from ε becomes larger with decreasing m_2. Assuming that diffusion of counterions ($\varepsilon_{\mathrm{LT,\ eff}}$) and the barrier against the diffusion of counterions ($\varepsilon_{\mathrm{LT,\ bar}}$) mainly contributes to ε, that is, $\varepsilon \approx \varepsilon_{\mathrm{LT,\ eff}} + \varepsilon_{\mathrm{LT,\ bar}}$, Fig. 12 suggests that at a given value of ε, $\varepsilon_{\mathrm{LT,\ eff}}(0) < \varepsilon_{\mathrm{LT,\ eff}}(5) < \varepsilon_{\mathrm{LT,\ eff}}(10)$, and thus $\varepsilon_{\mathrm{LT,\ bar}}(0) > \varepsilon_{\mathrm{LT,\ bar}}(5) > \varepsilon_{\mathrm{LT,\ bar}}(10)$. At a given ε, the values of $\Gamma^{\mathrm{H}}_{\mathrm{DTA}^+}$ increase with increasing m_2, the counterion binding χ goes up according to $\chi = 0.27\Gamma^{\mathrm{H}}_{\mathrm{DTA}^+}$, and thus, the surface charge density goes down. This effect leads to a decrease of the adsorption-desorption barrier against diffusion of counter ions. Therefore, it is likely that $\varepsilon_{\mathrm{LT,\ bar}}(0) > \varepsilon_{\mathrm{LT,\ bar}}(5) > \varepsilon_{\mathrm{LT,\ bar}}(10)$ and $D_{\mathrm{E}}(0) > D_{\mathrm{E}}(5)$ & $D_{\mathrm{E}}(10)$, although a quantitative analysis was not realized. To understand this feature, the ω vs $\Gamma^{\mathrm{H}}_{\mathrm{DTA}^+}$ and ε vs ω relations were constructed and are shown in Fig. 13a, b. Figure 13b shows that all the dilational elasticity vs $\Gamma^{\mathrm{H}}_{\mathrm{DTA}^+}$ curves, the adsorption-desorption barrier, and the diffusion coefficients were dependent on the concentration of the added salt. However, the value of the dilational elasticity itself was primarily determined by the ripplon frequency for a given surfactant DTABr even in the presence of added inorganic salt, at least, up to m_2/mmol kg^{-1} = 10.

In Fig. 14, τ_{eff} defined by Eq. 36 is plotted against $\Gamma^{\mathrm{H}}_{\mathrm{DTA}^+}$: it goes through unity at around the surface density of $\Gamma^{\mathrm{H,max}}_{\mathrm{DTA}^+}$, where ε passes through a maximum, for all cases of m_2/mmol kg^{-1} = 0, 5, and 10. When $\tau_{\mathrm{eff}} = 1$, the characteristic frequency of the counterion diffusion in the surface region $\omega_{\mathrm{dif,\ eff}}$ is equal to the ripplon frequency ω. Therefore, it can be said that because the ripplon frequency at the maximum ε is approximately 300 kHz from Fig. 13b, the diffusion of

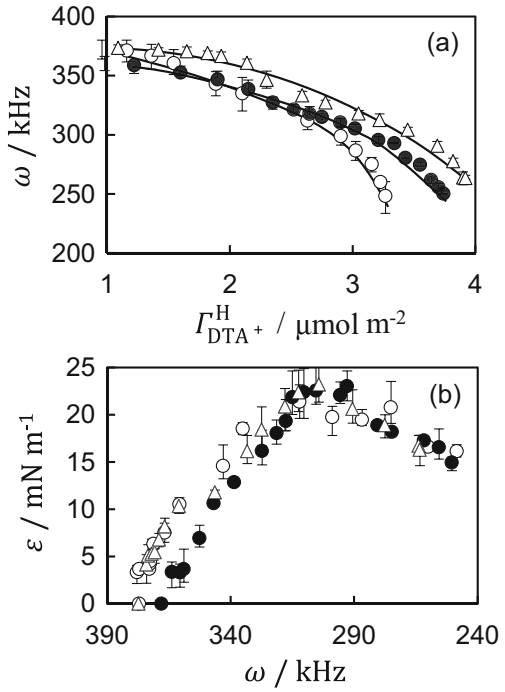

Fig. 13 **a** Ripplon frequency ω vs. surface density $\Gamma^{H}_{DTA^+}$ and **b** dilational elasticity ε vs. the ripplon frequency ω of DTABr at m_2 (mmol kg^{-1}) = 0 (○), 5 (●), and 10 (△)

counterions between the Stern and diffuse layers takes place on a time scale of 3.3 μs.

Dodecyltrimethylammonium ions with Br^-, BF_4^-, and SO_4^{2-}

The ε, ε_0, $\varepsilon_{LT,\ eff}$ vs $\Gamma^{H}_{DTA^+}$ curves are shown for $DTABF_4$ in Fig. 15a and DTA_2SO_4 in Fig. 15b. For BF_4^-, the value of $\varepsilon_{LT,\ eff}$ deviates from ε at the lower $\Gamma^{H}_{DTA^+}$ region, as was observed for Br^- (see Fig. 12). However, for SO_4^{2-}, the value of $\varepsilon_{LT,\ eff}$ was larger than that of ε at both lower and higher values of $\Gamma^{H}_{DTA^+}$ and was smaller in the intermediate $\Gamma^{H}_{DTA^+}$ range.

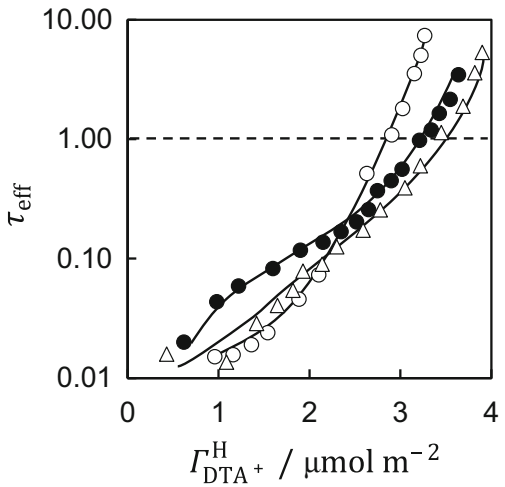

Fig. 14 τ_{eff} vs. surface density $\Gamma^{H}_{DTA^+}$ at m_2 (mmol kg^{-1}) = 0 (○), 5 (●), and 10 (△)

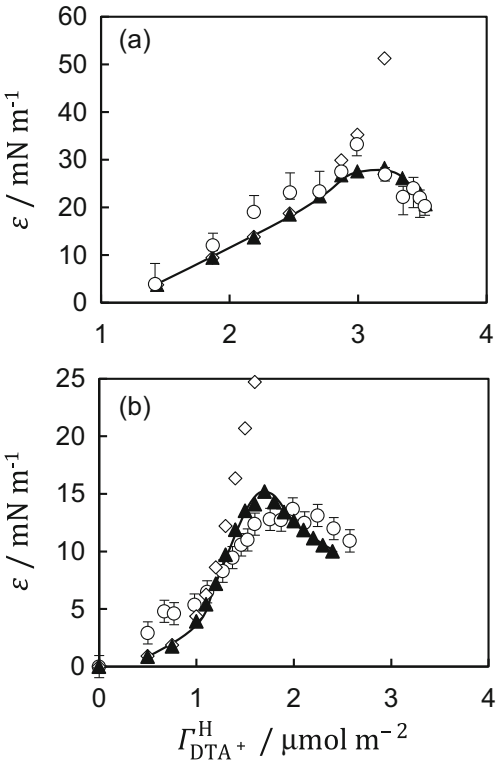

Fig. 15 Dilational elasticity vs. surface density $\Gamma^{H}_{DTA^+}$ curves of **a** $DTABF_4$, **b** DTA_2SO_4. ε from experiments (○), Gibbs elasticity ε_0 (◇), and effective LT model $\varepsilon_{LT,\ eff}$ (▲). Solid curves are guide to the eyes for $\varepsilon_{LT,\ eff}$

The D_E/m^2 s^{-1} values were $4.8 \times 10^{-9}(SO_4^{2-}) < 7.12 \times 10^{-8}(Br^-) < 4.4 \times 10^{-7}(BF_4^-)$. Because the D_E value is very different for different counterions, even for the same DTA^+ cation, and remains much higher than the diffusion coefficient of the DTA^+ ion, 6×10^{-10}m^2 s^{-1}, we conclude that the present SQELS study at high ripplon frequencies of 200–400 kHz provides information on both surfactant and counterion diffusion.

The ε vs $\Gamma^{H}_{DTA^+}$ curves are compared with each other in Fig. 16. It is clear that the maximum value of ε, ε^{max}, and the value of $\Gamma^{H}_{DTA^+}$ at ε^{max}, $\Gamma^{H,max}_{DTA^+}$, increased in the order of $BF_4^- > Br^- > SO_4^{2-}$. This order is the opposite to ordering of the magnitude of the dehydration free energy [62], i.e., $\Delta_{dehyd}G$/kJ mol^{-1} is: $190\ (BF_4^-) < 315(Br^-) < 1080(SO_4^{2-})$. The counterion binding to the surfactant ions generally becomes stronger as $\Delta_{dehyd}G$ decreases; hence, the tendency to escape from the Stern layer to the diffuse layer is accompanied by monolayer compression and this tendency is expected to become small. This expectation agrees with the findings in Fig. 16 that BF_4^- gives the highest ε^{max} and that D_E increases in the order: $4.8 \times 10^{-9}(SO_4^{2-}) < 7.12 \times 10^{-8}(Br^-) < 4.4 \times 10^{-7}(BF_4^-)$, as evaluated from the $\varepsilon_{LT,\ eff}$ fitting. Fig. 17a indicates that the dependence of ε on ω is clearly different for the different counterions. Conversely, the dependence is almost the same for

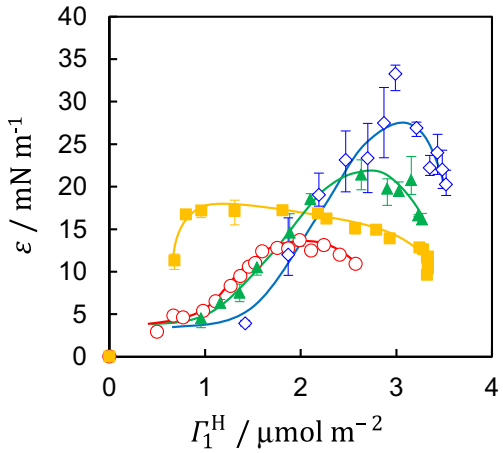

Fig. 16 Dilational elasticity ε vs surface density Γ_1^H curves of DTA_2SO_4 (○), DTABr (▲), $DTABF_4$ (◇), $C_{10}E_5$ (■)

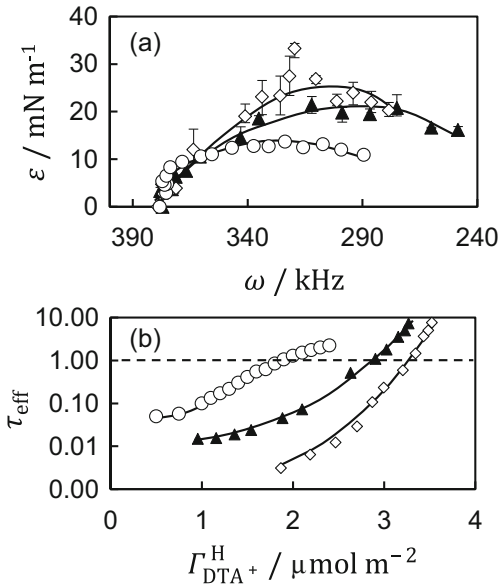

Fig. 17 **a** Dilational elasticity vs ripplon frequency and **b** τ_{eff} vs surface density for DTA_2SO_4 (○), DTABr (▲), and $DTABF_4$ (◇)

Br^- even in the presence of added salt, as shown in Fig. 13b. This finding confirms that the dilational elasticity estimated by SQELS at 200–400 kHz reflects the diffusion of counterions in the interfacial region and is determined not only by the perturbation (ripplon) frequency but also by the strength of binding of the counterion to the surfactant ion. The τ_{eff} vs $\Gamma_{DTA^+}^H$ curves given in Fig. 17b show that at $\Gamma_{DTA^+}^{H,max}$, τ_{eff} passes through unity, and thus, the characteristic frequency of the diffusion $\omega_{dif.\ eff}$ is equal to the ripplon frequency ω. The results in Fig. 17a, give $\omega_{dif.\ eff}$ values of approximately 300 kHz (Br^-), 310 kHz (BF_4^-), 320 kHz (SO_4^{2-}). Thus, the time scale of counterion diffusion is estimated to be in the range of 3.3 – 3.1 μs.

SQELS studies of nonionic surfactants with oxyethylene units ($C_{10}E_5$)

In the above section with respect to cationic surfactants, we demonstrated that relaxation processes relevant to high frequency ripplons are not related to diffusion of surfactant ions but rather to diffusion of counter ions in the interfacial region. Although the transfer of counterions between the Stern layer and diffuse layer generally accompanies hydration-dehydration of counterions, it is practically impossible to treat the influence of counterions and water on dilational elasticity separately. To know how water molecules influence the dilational elasticity in the high frequency regions, the SQELS studies were adapted to the adsorbed monolayers of nonionic surfactants with oxyethylene units, $CH_3(CH_2)_9(OCH_2CH_2)_5OH$, abbreviated as $C_{10}E_5$.

The ε vs $\Gamma_{C_{10}E_5}^H$ plot of this system shows a notable difference from those of the ionic surfactants, as shown in Fig. 16. For example, $\Gamma_{C_{10}E_5}^{H,max}$ is approximately 1 μmol m^{-2} and much smaller than the saturation adsorption (~3.3 μmol m^{-2}). Additionally, the value of ε decreases slowly over a wide range of $\Gamma_{C_{10}E_5}^H$ above $\Gamma_{C_{10}E_5}^{H,max}$ as compared with the behavior of the ionic surfactants, suggesting a different relaxation mechanism for the $C_{10}E_5$ surfactants. The ε values are plotted against $\Gamma_{C_{10}E_5}^H$ together with curves of ε^0, ε_{LT}, ε_{MLT}, and $\varepsilon_{LT,\ eff}$ in Fig. 18, where $D/m^2\ s^{-1} = 4.30 \times 10^{-10}$ and $k_d/mol\ m^{-2}s^{-1} = 4.25 \times 10^{-4}$ were used [56, 57]. It should be noted that ε_{LT} based on the diffusion coefficient of $C_{10}E_5$ in aqueous solution D is almost equal to ε_0 and does not trace ε even at higher surface densities where the diffusion of surfactant molecules is expected to be influential. The ε_{MLT} values calculated from Eq. 34 coincide with ε_0 perfectly as expected at high frequencies for case 4. These observations derive from the conclusion that the relaxation affecting the dilational elasticity is not attributable to diffusion of $C_{10}E_5$ molecules but to some processes relevant to the water molecules.

Because even $\varepsilon_{LT,\ eff}$ largely deviates from ε over a wide range of $\Gamma_{C_{10}E_5}^H$, the examination on the basis of the diffusion models is not realistic. As a possible qualitative explanation, the cross-sectional area of even a non-hydrated hydrophilic group is approximately 0.23 nm^2 and considerably larger than that of a hydrocarbon chain (0.18 nm^2). Thus, the hydrated hydrophilic groups are expected to be sitting closer to each other than the hydrophobic chains even for small $\Gamma_{C_{10}E_5}^H$. When regions with a higher local surface density (HLSD) of lower local surface tension and those with a lower surface density (LLSD) of higher local surface tension, relative to the equilibrium situation, are created by the capillary wave, the possible relaxation processes include distortion of the hydration sphere and/or hydration-dehydration of the hydration sphere caused by diffusion of water molecules. It seems probable that at a lower $\Gamma_{C_{10}E_5}^H$, only the distortion responds to ripplon perturbation. However, at a higher $\Gamma_{C_{10}E_5}^H$, the results

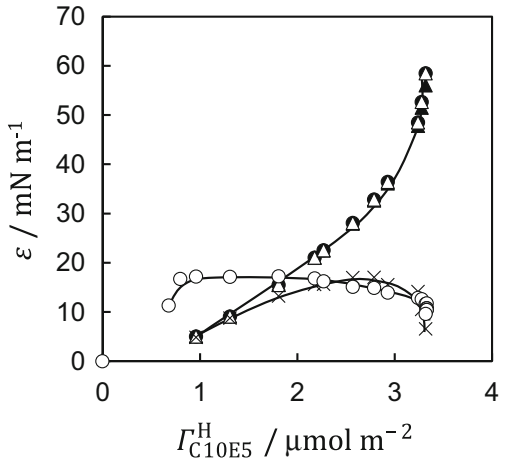

Fig. 18 Comparisons among the dilational elasticities obtained from experiments and models for $C_{10}E_5$. ε from experiments (○), Gibbs elasticity ε_0 (●), LT model ε_{LT} (▲), MLT model ε_{MLT} (△), effective LT model $\varepsilon_{LT,\ eff}$ (×)

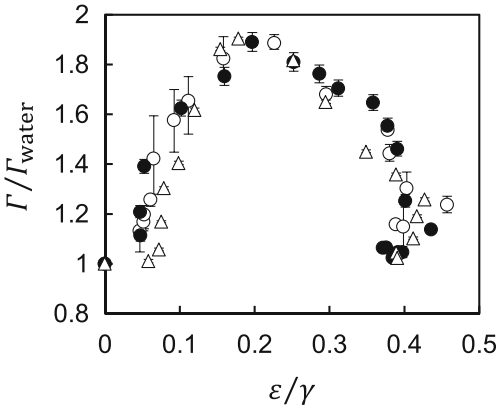

Fig. 19 Loss modulus $\omega\kappa$ and damping coefficients Γ/Γ_{water} plotted against ε/γ for the DTABr-NaBr mixtures at m_2 (mmol kg^{-1}) = 0 (○), 5 (●), and 10 (△)

suggest that the hydrophilic part of the monolayer is dehydrated to some extent [63], hydration-dehydration processes are essential for inducing perturbations in ripplons. Assuming that the ripplon frequency at the surface density $\Gamma^{H,max}_{C_{10}E_5}$ giving ε^{max} corresponds to the characteristic frequency for diffusion of water, $\omega_{dif.\ eff}$, as is the case for an ionic surfactant, the frequency is estimated to be approximately 310 kHz. Because the ripplon frequency above $\Gamma^{H,max}_{C_{10}E_5}$ decreases to approximately 210 kHz at the saturated adsorption, we expected that the dehydration-hydration caused by diffusion of water molecules has a strong influence on ε. This expectation is consistent with the fact that $\varepsilon_{LT,\ eff}$ becomes comparatively close to ε at high $\Gamma^{H}_{C_{10}E_5}$.

There have been some reports on the dilational elasticity of C_iE_j surfactants. Ravera et al. demonstrated that for $C_{10}E_4$ surfactant adsorption, the characteristic frequency for diffusion is approximately 0.4 Hz, while that for surfactant reorientation is approximately 800 Hz [3]. This result supports our finding that the relaxation process captured by SQELS at ripplon frequencies of several hundred kHz is neither related to surfactant diffusion nor to surfactant reorientation. Sharpe and Eastoe [21] reported a dilational elasticity in the range of 20–30 mN m^{-1} as a function of ripplon frequency from 30 to 90 kHz for $C_{10}E_8$ and $C_{12}E_5$, which roughly coincides with ε^{max} of the present study.

Damping coefficients

The damping coefficient evaluated from phenomenological fitting is plotted against ε/γ for DTABr at m_2/mmol kg^{-1}= 0, 5, and 10 in Fig. 19, which clearly demonstrates that Γ/Γ^{max} has a maximum in the range of $\varepsilon/\gamma \approx 0.15-0.2$. Because $\omega\kappa$ was shown to take a negative value at approximately ε/γ~0.1, such a negative viscosity closely correlates with resonance between the transversal and dilational waves [64].

Eastoe et al. measured the surface dilational viscoelasticity of aqueous solutions of hexadecyltrimethylammonium bromide (HTABr) with and without dodecane (C12) by the SQELS method and found that the sign of κ switched from negative to positive through the addition of C12 [27]. Monroy et al. also found negative dilational viscosities for HTABr from the ECW experiments [17] and reported that such negative dilational viscosities arise from deficiencies in the hydrodynamic description of the interface and an appropriate dispersion equation of interface is absolutely necessary [23]. The amplitude of the capillary wave τ estimated by $<\tau^2>^{1/2} = \sqrt{(kT/(\gamma q^2 + \rho g)}$ was 0.2–0.5 nm at a surface tension γ of the aqueous DTAB solution. Conversely, the interface thickness (Debye length) estimated from the Gouy–Chapmann distribution was 8–2.5 nm in the absence of NaBr and 3–2 nm at a NaBr concentration of 10 mM for the aqueous DTAB solutions. Furthermore, the thickness of the counterion distribution, including the surface roughness, was estimated to be approximately 1.1 nm from X-ray reflectivity measurements [65]. Therefore, although the amplitude of the capillary wave might be somewhat smaller than the interface thickness, there is every possibility that the capillary deformation of the interface brings the monolayer into contact with the bulk region. In those cases, an additional coupling term should be incorporated into the dispersion equation as described by Monroy et al. [23], Thominent et al. [28], and Hennenberg et al. [22]. Furthermore, the model proposed by Bonfillon and Langevin is likely more sophisticated than the usual MLT model for charged surfactants [19].

To improve our understanding of these systems further theoretical and experimental studies are needed. In particular, we need more experiments on ionic surfactants in the presence of added inorganic salts at higher concentrations than those used in the present study. Furthermore, mixtures of different ionic surfactants with hydrocarbons and different types of nonionic

compounds of the form C_iE_j should be investigated and analyzed using different useful models. Our future SQELS studies will focus on these aspects.

Conclusions

The surface dilational viscoelasticities of aqueous solutions of short chain lipid mixtures, cationic surfactants with different counterions, and nonionic surfactants with oxyethylene units were investigated by measuring SQELS spectra and analyzing these data by both surface rheological and phenomenological fitting. The evaluated dilational elasticities were examined by the Lucassen-van den Temple model and its analogues.

From the ECW and SQELS studies on the lipid mixtures, we demonstrated that the molecular interaction between DC_8PC and DC_6PC in the adsorbed film clearly influenced the relaxation process on the order of milliseconds (ECW); however, these interactions were not so influential on relaxation of the order of microseconds (SQELS). The frequency dependence of the dilational viscoelasticity with the use of ECW suggested that the characteristic frequencies for relaxation from staggered structure formation were likely in the range from 150 to 300 Hz. Thus, the time scale was of the order of milliseconds.

The dilational elasticity of cationic surfactants with different counterions were evaluated from SQELS studies at 250–400 kHz and examined using the LT, modified LT, and effective LT models. Examination of the DTABr adsorbed film suggested that the main influential relaxation processes on the dilational property at this high frequency were neither related to diffusion of surfactant from the bulk phase to the subsurface nor an adsorption-desorption of surfactant ions between the adsorbed layer and subsurface. Rather, the most influential factors related to diffusion of counter ions taking place in the interfacial region owing to capillary wave dilation. This was confirmed from studies on the DTABr and NaBr system, which showed that the value of dilational elasticity itself was primarily determined by the ripplon frequency for a given surfactant, DTABr. This case was true even in the presence of added inorganic salt and the diffusion of counterions between the Stern and diffuse layers takes place on a time scale of 3.3 μs. Moreover, investigations on the $DTABF_4$ and DTA_2SO_4 systems revealed that the order of the change in magnitude of the diffusion coefficient in the interfacial region coincided with the degree of counterion binding to surfactant cation and dehydration energy. This result confirms the suggestion that the most influential relaxation processes on the dilational property were related to counterion diffusion in the interfacial region.

The SQELS studies of nonionic surfactants with oxyethylene units ($C_{10}E_5$) showed that neither the LT, modified LT, nor effective LT models could completely follow the experimental dilational elasticity. However, it was suggested that the relaxation process captured by the SQELS studies at ripplon frequencies of several hundred kHz were neither related to surfactant diffusion nor to surfactant reorientation. Rather, the possible relaxation processes were related to distortion of the hydration sphere and/or hydration-dehydration to/from hydration sphere caused by diffusion of water molecules.

Finally, negative values of surface dilational viscosity were also found. We concluded that Γ/Γ^{max} has a maximum at approximately $\varepsilon/\gamma \approx 0.15$~$0.2$ and $\omega\kappa$ starts to take a negative value around ε/γ~0.1. Therefore, such negative viscosity might be closely related to the resonance between the transversal and dilational waves.

The present SQELS studies could provide information on the diffusion of counterions and water molecules in the interfacial region. The conclusions given above should be examined further using other types of ionic and nonionic surfactants, surfactant mixtures. Nevertheless, we showed that SQELS studies are capable of capturing useful and interesting information, which other methods at lower frequencies do not provide.

Acknowledgements The authors would like to express their gratitude to Prof. Y. Ohmasa (Kansai University) for his support of our analytical techniques, Prof. K. Sakai (University of Tokyo) for his support constructing the SQELS apparatus, and Prof. R.G. Rubio, Prof. F. Ortega and Dr. A M. Martin (Universidad Complutense de Madrid) for permission to perform the ECW experiments at their laboratory. M. A. also would like to thank Mr. S. Matsubara (Kyushu University) for his extensive calculations of the relevant quantities used in the models. We thank Andrew Jackson, PhD, from Edanz Group (www.edanzediting.com/ac) for editing a draft of this manuscript.

Funding information This work was supported in part by the Grant-in-Aid for Scientific Research (B) and (C) of Japan Society for the Promotion of Science (no. JP21350078 and no. JP17K05837).

Compliance with ethical standards

Conflict of interest The authors declare that they have no conflict of interest.

References

1. Langevin D (1998) Dynamics of surfactant layers. Curr Opin Colloid Interface Sci 3(6):600–607. https://doi.org/10.1016/S1359-0294(98)80086-1
2. Eastoe J, Dalton JS (2000) Dynamic surface tension and adsorption mechanisms of surfactants at the air/water interface. Adv Colloid Interf Sci 85(2–3):103–144. https://doi.org/10.1016/S0001-8686(99)00017-2
3. Ravera F, Ferrari M, Santini E, Liggieri L (2005) Influence of surface processes on the dilational visco-elasticity of surfactant solutions. Adv Colloid Interf Sci 117(1–3):75–100. https://doi.org/10.1016/j.cis.2005.06.002

4. Monroy F, Ortega F, Rubio RG, Velarde MG (2007) Surface rheology, equilibrium and dynamic features at interfaces, with emphasis on efficient tools for probing polymer dynamics at interfaces. Adv Colloid Interf Sci 134-135:175–189. https://doi.org/10.1016/j.cis.2007.04.023
5. Miller R, Liggeri L (2010) Interfacial rheology-the response of two-dimensional layers on external perturbations. Curr Opin Colloid Interface Sci 15(4):215–216. https://doi.org/10.1016/j.cocis.2010.05.001
6. Mucic N, Javadi A, Kovalchuk NM, Aksenenko EV, Miller R (2011) Dynamics of interfacial layers—experimental feasibilities of adsorption kinetics and dilational rheology. Adv Colloid Interf Sci 168(1–2):167–178. https://doi.org/10.1016/j.cis.2011.06.001
7. Lofti M, Karbaschi M, Javadi A, Mucic N, Krägel J, Kovalchuk VI, Rubio RG, Fainerman VB, Miller R (2014) Dynamics of liquid interfaces under various types of external perturbations. Curr Opin Colloid Interface Sci 19(4):309–319. https://doi.org/10.1016/j.cocis.2014.04.006
8. Georgieva D, Schmitt V, Leal-Calderon F, Langevin D (2009) On the possible role of surface elasticity in emulsion stability. Langmuir 25(10):5565–5573. https://doi.org/10.1021/la804240e
9. Bergeron V (1997) Disjoining pressures and film stability of alkyltrimethylammonium bromide foam films. Langmuir 13(13):3474–3482. https://doi.org/10.1021/la970004q
10. Delacotte J, Montel L, Restangno F, Scheid B, Dollet B, Stone HA, Langevin D, Rio E (2012) Plate coating: influence of concentrated surfactants on the film thickness. Langmuir 28(8):3821–3830. https://doi.org/10.1021/la204386b
11. Lópen-Montero I, Mateos-Gil P, Sferrazza M, Navajas PL, Rivas G, Vélez M, Monroy F (2012) Active membrane viscoelasticity by the bacterial FtsZ-division protein. Langmuir 28(10):4744–4753. https://doi.org/10.1021/la204742b
12. Cicuta P, Hopkinson I (2004) Recent developments of surface light scattering as a tool for optical-rheology of polymer monolayers. Colloids Surf A Physicochem Eng Asp 233(1–3):97–107. https://doi.org/10.1016/j.colsurfa.2003.11.025
13. Langevin D (1981) Light scattering study of monolayer viscoelasticity. J Colloid Interface Sci 80(2):412–425. https://doi.org/10.1016/0021-9797(81)90200-9
14. Maru HC, Wasan DT (1979) Dilational viscoelastic properties of fluid interfaces-II. Exp Study Chem Eng Sci 34(11):1295–1307. https://doi.org/10.1016/0009-2509(79)80021-4
15. Stubenrauch C, Fainermann VB, Aksenenko V, Miller R (2005) Adsorption behavior and dilational rheology of the cationic alkyl trimethylammonium bromides at the water/air interface. J Phys Chem B 109(4):1505–1509. https://doi.org/10.1021/jp046525l
16. Liggieri L, Miller R (2010) Relaxation of surfactants adsorption layers at liquid interfaces. Curr Opin Colloid Interface Sci 15(4):256–263. https://doi.org/10.1016/j.cocis.2010.02.003
17. Monroy F, Kahn JG, Langevin D (1998) Dilational viscoelasticity of surfactant monolayers. Colloids Sur A 143(2–3):251–260. https://doi.org/10.1016/S0927-7757(98)00373-2
18. Stenvot C, Langevin D (1988) Study of viscoelasticity of soluble monolayers using analysis of propagation of excited capillary waves. Langmuir 4(5):1179–1183. https://doi.org/10.1021/la00083a022
19. Bonfillon A, Langevin D (1994) Electrostatic model for the viscoelasticity of ionic surfactant monolayers. Langmuir 10(9):2965–2971. https://doi.org/10.1021/la00021a020
20. Earnshaw JC, McCoo E (1995) Surface light-scattering studies of surfactant solutions. Langmuir 11(4):1087–1100. https://doi.org/10.1021/la00004a011
21. Sharpe D, Eastoe J (1996) Properties of surfactant monolayers studied by surface light scattering. Langmuir 12(9):2303–2307. https://doi.org/10.1021/la951078+
22. Hennenberg M, Slavtchev S, Weyssow B, Legros JC (2000) On the Earnshaw and the Van den Tempel–Lucassen compositional viscoelastic theories. J Colloid Interface Sci 230(1):216–218. https://doi.org/10.1006/jcis.2000.7099
23. Monroy F, Munoz MG, Rubio JEF, Ortega F, Rubio RG (2002) Capillary waves in ionic surfactant solutions: effects of the electrostatic adsorption barrier and analysis in terms of a new dispersion equation. J Phys Chem B 106(22):5636–5644. https://doi.org/10.1021/jp012044f
24. Takajo Y, Yamanaka M, Rubio RG, Takiue T, Matsubara H, Aratono M (2013) Synergistic interaction of short-chain phospholipids in the adsorbed film and micelles: study by surface tension and dilational viscoelasticity measurements. J Phys Chem C 117(2):1097–1104. https://doi.org/10.1021/jp311283a
25. Aratono M, Uryu S, Hayami Y, Motomura K, Matuura R (1984) Phase transitions in the adsorbed films at water/air interface. J Colloid Interface Sci 98(1):33–38. https://doi.org/10.1016/0021-9797(84)90475-2
26. Takiue T, Kawagoe Y, Muroi S, Murakami R, Ikeda N, Aratono M, Tanida H, Sakane H, Watanabe I (2003) Surface density measurement of the bromide ion by the total-reflection X-ray absorption fine structure technique at the air/aqueous dodecyltrimethylammonium bromide solution interface. Langmuir 19(26):10803–10807. https://doi.org/10.1021/la0300582
27. Eastoe J, Sharpe D (1998) Surface light scattering from cationic surfactant films. Colloids Surf A Physicochem Eng Asp 143(2–3):261–271. https://doi.org/10.1016/S0927-7757(98)00260-X
28. Thominet V, Stenvot C, Langevin D (1988) Light scattering study of the viscoelasticity of soluble monolayers. J Colloid Interface Sci 126(1):54–62. https://doi.org/10.1016/0021-9797(88)90098-7
29. Li HH, Imai Y, Yamanaka M, Hayami Y, Takiue T, Matsubara H, Aratono M (2011) Specific counterion effect on the adsorbed film of cationic surfactant mixtures at the air/water interface. J Colloid Interface Sci 359(1):189–193. https://doi.org/10.1016/j.jcis.2011.03.082
30. Imai Y, Shimamoto K, Takiue T, Matsubara H, Aratono M (2010) Study on surface adsorption from cationic surfactant–electrolyte mixed aqueous solution including BF_4^- ion. Colloid Polym Sci 288(9):1005–1011. https://doi.org/10.1007/s00396-010-2221-y
31. Li HH, Imai Y, Takiue T, Matsubara H, Aratono M (2013) Effect and mixing of counter anions at the surface of aqueous solution of imidazolium-based ionic liquids. Colloids Surf A Physicochem Eng Asp 427:26–32. https://doi.org/10.1016/j.colsurfa.2013.02.062
32. Matsubara H, Onohara A, Imai Y, Shimamoto K, Takiue T, Aratono M (2010) Effect of temperature and counterion on adsorption of imidazolium ionic liquids at air–water interface. Colloids Surf A Physicochem Eng Asp 370(1–3):113–119. https://doi.org/10.1016/j.colsurfa.2010.08.057
33. Imai Y, Li HH, Takumi H, Tanida H, Watanabe I, Takiue T, Matsubara H, Aratono M (2012) Study on the distribution of binary mixed counterions in surfactant adsorbed films by total reflection XAFS measurements. J Colloid Interface Sci 388(1):219–224. https://doi.org/10.1016/j.jcis.2012.08.044
34. Shimamoto K, Onohara A, Takumi H, Watanabe I, Tanida H, Matsubara H, Takiue T, Aratono M (2009) Miscibility and distribution of counterions of imidazolium ionic liquid mixtures at the air/water surface. Langmuir 25(17):9954–9959. https://doi.org/10.1021/la901114e
35. Motomura K (1978) Thermodynamic studies on adsorption at interfaces. I. General formulation. J Colloid Interface Sci 64(2):348–355. https://doi.org/10.1016/0021-9797(78)90371-5
36. (1992) Light scattering by liquid surfaces and complementary techniques. In: D Langevin (ed) Surfactant science series, vol 41. Marcel Dekker, New York
37. Lucassen-Reynders EH, Lucassen J (1969) Properties of capillary waves. Adv Colloid Interface Sci 2(4):347–395. https://doi.org/10.1016/0001-8686(70)80001-X

38. Lucassen J, van den Temple M (1972) Dynamic measurements of dilational properties of a liquid interface. Chem Eng Sci 27(6): 1283–1291. https://doi.org/10.1016/0009-2509(72)80104-0
39. van den Temple M, Lucassen-Reynders EH (1983) Relaxation processes at fluid interfaces. Adv Colloid Interf Sci 18(3–4):281–301. https://doi.org/10.1016/0001-8686(83)87004-3
40. Schubert K, Strey R, Kahlweit M (1991) A new purification technique for alkyl polyglycol ethers and miscibility gaps for water-C_iE_j. J Colloid Interface Sci 141(2):21–29. https://doi.org/10.1016/0021-9797(91)90298-M
41. Motomura K, Aratono M (1987) Geometric formalism of the thermodynamics of adsorption at interfaces between two fluid phases. Langmuir 3(2):304–306. https://doi.org/10.1021/la00074a029
42. Sakai K, Honda H, Hiraoka Y (2005) Rapid ripplon spectroscopy with ms time resolution. Rev Sci Instrum 76(6):063908. https://doi.org/10.1063/1.1928172
43. Sakai K, Takagi K (1994) Ripplon spectroscopic study on relaxation of surface viscoelasticity in soluble monolayers on surfactant solutions. Langmuir 10(1):257–261. https://doi.org/10.1021/la00013a038
44. Sakai K, Takagi K (1992) Relaxation of 2-dimensional viscoelasticity in a long-chain fatty acid monolayer expanded at the air-water interface. Jpn J Appl Phys 31(2):L1488–L1491. https://doi.org/10.1143/JJAP.31.L1488
45. Monroy F, Ortega F, Rubio RG (1998) Dilational rheology of insoluble polymer monolayers: poly(vinylacetate). Phys Rev E 58(6): 7629–7641. https://doi.org/10.1103/PhysRevE.58.7629
46. Kramer L (1971) Theory of light scattering from fluctuations of membranes and monolayers. J Chem Phys 55(5):2097–2105. https://doi.org/10.1063/1.1676380
47. Ohmasa Y, Hoshino T, Osada R, Yao M (2008) Surface waves at the liquid–vapor interface of ionic liquid [bmim][TFSI]. Chem Phys Lett 455(4–6):184–188. https://doi.org/10.1016/j.cplett.2008.02.077
48. Richards RW, Rochford BR, Taylor MR (1996) Surface quasi-elastic light scattering from spread monolayers of a poly(methyl methacrylate)−poly(ethylene oxide) block copolymer. Macromolecules 29(6):1980–1991. https://doi.org/10.1021/ma950853p
49. Sharpe D, Earnshaw JC (1997) Surface viscoelastic relaxation on aqueous solutions of tetrahydrofuran. J Chem Phys 107(18):7493–7501. https://doi.org/10.1063/1.474989
50. Aumaitre E, Wongsuwarn S, Rossetti D, Hedges ND, Cox AR, Vella D, Cicuta PA (2012) Viscoelastic regime in dilute hydrophobin monolayers. Soft Matter 8:1175–1183. https://doi.org/10.1039/C1SM06139A
51. Kizling J, Stenius P, Eriksson JC, Ljunggren S (1995) Viscoelastic properties of dodecylammonium chloride monolayers. J Colloid Interface Sci 171(2):162–167. https://doi.org/10.1006/jcis.1995.1162
52. Earnshaw JC, McLaughlin AC (1991) Waves at liquid surfaces-coupled oscillations and mode mixing. Proc R Soc Lond A 433(1889):663–678. https://doi.org/10.1098/rspa.1991.0069
53. Earnshaw JC, McLaughlin AC (1993) Waves at liquid surfaces II. Surfactant action and coupled oscillators. Proc R Soc Lond A 440(1910):519–536. https://doi.org/10.1098/rspa.1993.0031
54. Munoz MG, Luna L, Monroy F, Rubio RG, Ortega F (2000) Viscoelastic behavior of 1-dodecanol monolayers undergoing a liquid-solid phase transition. A surface quasielastic light scattering study. Langmuir 16(16):6657–6666. https://doi.org/10.1021/la0001474
55. Lucassen J, van den Tempel M (1972) Longitudinal waves on visco-elastic surfaces. J Colloid Interface Sci 41(3):491–498. https://doi.org/10.1016/0021-9797(72)90373-6
56. Lucassen J, Hansen RS (1967) Damping of waves on monolayer-covered surfaces: II Influence of Bulk-to-Surface Diffusional Interchange on Ripple Characteristics. J Colloid Interface Sci 23(3):319–328. https://doi.org/10.1016/0021-9797(67)90175-0
57. Li B, Geeraerts G, Joos P (1994) Kinetic equations for transfer-controlled adsorption kinetics. Colloids Surfaces A 88(2–3):251–266. https://doi.org/10.1016/0927-7757(94)02791-9
58. Eastoe J, Dalton JS, Rogueda PGA, Crooks ER, Pitt AR, Simister EA (1997) Dynamic surface tensions of nonionic surfactant solutions. J Colloid Interface Sci 188(2):423–430. https://doi.org/10.1006/jcis.1997.4778
59. CRC HANDBOOK OF CHEMISTRY and PHYSICS 87th EDITION
60. Weingartner H (1982) Self diffusion in liquid water. A reassessment. Z Phys Chem NF(Leiptig) 132(2):129–149. https://doi.org/10.1524/zpch.1982.132.2.129
61. Imai Y (2014) Specific ion effect on counterion distribustion in surfactant adsorbed films studied through surface tensiometry and total reflection XAFS, Ph.D thesis (Kyushu University)
62. Marcus Y (1994) A simple empirical model describing the thermodynamics of hydration of ions of widely varying charges, sizes, and shapes. Biophys Chem 51(2–3):111–127. https://doi.org/10.1016/0301-4622(94)00051-4
63. Wongwailikhit K, Ohta A, Seno K, Nomura A, Shinozuka T, Takiue T, Aratono M (2001) Temperature effect on the adsorption and micelle formation of pentaethylene glycol monoalkyl ethers. J Phys Chem B 105(46):11462–11467. https://doi.org/10.1021/jp011886b
64. Giermanska-Kahn J, Monroy F, Langevin D (1999) Negative effective surface viscosities in insoluble fatty acid monolayers: effect of phase transitions on dilational viscoelasticity. Phys Rev E 60(6): 7163–7173. https://doi.org/10.1103/PhysRevE.60.7163
65. Matsubara H, Takaichi T, Takiue T, Tanida H, Uruga T, Yano Y, Aratono M (2013) X-ray reflectivity measurements for freezing transitions of alkane wetting film on surfactant solution surface. Bull Chem Soc Jpn 86(4):492–496. https://doi.org/10.1246/bcsj.20120263